N° d'ordre : 00002/94

THESE PRESENTEE POUR OBTENIR LE GRADE DE DOCTEUR EN SCIENCES DE L'UNIVERSITE NATIONALE DU BENIN

Option : **Physique**

par

Jean B. CHABI OROU

Sujet : **The Evolution of Vorticity in a Free Shear Layer with Compressible Turbulence And A Theory of Homogeneous Condensation.**

Soutenue le 25 Mai 1994 devant le JURY :

Président : **André BELLEMANS** (Université Libre de Bruxelle-Belgique)

Rapporteurs : **Christian DIATTA** (Université de Dakar Sénégal)

Roger Paul HAZOUME (Université Nationale du Bénin)

Joseph A JOHNSON III (Florida A & M University, Tallahassee, Florida, USA)

Examinateurs : **Abel AFOUDA** (Université Nationale du Bénin)

Moussiliou GBADAMASSI (Université Nationale du Bénin)

Co - Directeurs : ROGER PAUL HAZOUME

JOSEPH A. JOHNSON III

Remerciements

Je voudrais tout d'abord remercier le Professeur André BELLEMANS pour l'honneur qu'il me fait en acceptant de présider le jury de ma thèse. Mes remerciements vont également aux Professeurs Abel AFOUDA, Christian DIATTA et Moussiliou GBADAMASSI qui ont accepté d'être membre de ce jury.

Je tiens également à remercier l'Université Nationale du BENIN (UNB) , le "Centre International de Physique Théorique" de Trieste (Italie), le "department of Physics" du "City College of City University of New-York" aux USA puis le "Center for Nonlinear and Nonequilibrium Aeroscience" (CeNNAs) du "Florida A&M University " de Tallahassee en Floride aux USA et l'Institut de Mathématiques et de Sciences Physiques (IMSP) pour leurs appuis financier, matériel et moral .

Les Professeurs Joseph A. JOHNSON III, Directeur du CeNNAs et Roger P. HAZOUME de l'UNB ont manifesté leur intérêt, disponibilité, patience et compréhension dans le choix et la conduite de ces sujets de thèse. Qu'ils trouvent ici l'expression de mes profonds remerciements.

Au CeNNAs, j'ai travaillé avec une équipe de chercheurs et d'amis sincères dont le Dr Ronald WILLIAMS qui m'a beaucoup aidé avec les autres étudiants du centre et Ms Stephanie HUMPHRIES avec qui j'ai étudié l'influence de la température sur les courbes de calibrage de la fluorescence induite par le laser sur les molécules de dioxyde d'azote.

Je ne manquerai pas de citer Dr Lynette E. JOHNSON, Directrice Adjointe du CeNNAs qui a tenu à participer en personne à la soutenance de cette thèse.
Je les remercie sincèrement pour leur acte d'amour profond sans oublier les autres membres du personnel de ce laboratoire.

Que les professeurs Ambroise ADISSIN et Victor HOUNDONOUGBO de l'UNB et leurs familles respectives trouvent ici l'expression de mes profonds remerciements pour leurs encouragements et soutiens permanents .

Mr Etienne KOSSI, Ingénieur des télécommunications à l'OPT et sa famille m'ont soutenu tout au long de ce parcours, qu'ils trouvent ici, en même temps que les autres restés dans l'anonymat, l'expression de ma profonde gratitude.

Je loue tout particulièrement ici le reconfort chaleureux et permanent que mon épouse Mme Amina O. CHABI née SARRE, mes enfants et mes parents n'ont cessé de m'apporter. Je leur dis à tous merci de tout coeur.

Enfin, je remercie le Directeur de l'IMSP, le Professeur Jean-Pierre EZIN, les enseignants et les étudiants de l'IMSP qui ont été les vrais artisans de la réalisation de ce travail.

Table of contents

Part A

Part B

Part A

THE EVOLUTION OF VORTICITY IN A FREE SHEAR LAYER WITH COMPRESSIBLE TURBULENCE

Abstract

A supersonic Ludwieg tube is used to produce a free shear with compressible turbulence. Resonance radiation from Laser Induced Fluorescence provides a calibrated density diagnostic. A new experimental procedure affords the implementation of a Direct Velocity Estimation technique based on a large scale one-dimensional approximation to the Navier-Stokes equations. Strong velocity fluctuation bursts have been observed in the free shear layer. They suggest an important role for velocity gradients in this flow regime.

When $\nabla . U \neq 0$, free shear layers with compressible turbulence can show a sensitivity of second viscosity to Reynolds number. Using a dominant mode approach, a resonance-like behavior for vorticity fluctuations is calculated.

List of figures

I. Introduction

Recently it is found (Brown & Roshko)[1] that a mixing layer is dominated by large scale coherent vortical structures. Brown and Roshko have studied the effect of density fluctuations on the growth rate of mixing layers. They found that density effects alone cannot explain the slow growth rate of the supersonic shear layer. The effect of flow compressibility on turbulence is of interest in many applications including high-speed external flow and supersonic combustion. In astrophysics, chemical reactions, drag and noise reduction there is an intense interest in effect of compressiblity.

Another study [2] of the compressible shear layer showed that the compressibility effects indeed play a dominant role in the slow growth rate of the layer. In high Mach number fluid flows, compressibility is also apparently important in the formation of coherent structures; their interaction with surrounding environment seems to be the cause of a subsequent generation of transient shock waves known as shocklets. It is speculated that these structures in compressible flow are associated with the generation of the vorticity in the fully developed turbulent flow. Other studies have linked the decreased growth rate at supersonic convective Mach numbers to the existence of shocks and shocklets [3]. Therefore the shocklets were assumed to hinder the growth rate by both the production of counter vorticity, and by reducing the turbulence scales. The turbulent motion is therefore to be composed of various sized eddies (and their associated frequencies) which have a certain kinetic energy determined by their vorticity or by the intensity of the velocity fluctuation of the corresponding frequency.

However, none of these speculations have been reported. Specially, there is the question of the distribution of kinetic energy of turbulence among the various frequencies. It is possible on the average, to allocate a certain amount of the total energy to a distinct frequency. Turbulent motion can be assumed to consist of the superposition of eddies of various sizes and vorticities with distinguishable upper and lower limits. From this perspective, the upper size limit of the eddies should be determined mainly by the size of the apparatus in which the flow is taking place whereas the lower limit is determined by viscosity effects and decreases with increasing velocity of the average flow. Thus, at high Reynolds number, the role of the viscosity effects might couple directly into the turbulent energy deposition mechanisms, therefore, one can see how the vorticity measurement in compressible flow can lead to the understanding of turbulence phenomenon in regimes with strong spectral modes; one also sees an important role which rotational effects in nonequilibrium turbulent environment might play on the evolution of viscosity.

This dissertation research is intended to address this need. There will be a general focus on phenomena driven by velocity gradients and velocity fluctuations. A determination has been made, first of all, of the relationship between the influence of nonequilibrium relaxation on the evolution of second viscosity. A relationship has been established between the second viscosity, turbulence and the relaxation time for a nonequilibrium process. In addition, a new well calibrated technique using laser induced fluorescence for direct velocity estimates from density time histories has been proven so as to allow the evolution of vorticity on the axis of a supersonic free shear layer to be measured. Dominant modes seem to play an important role in certain regimes of supersonic turbulent flow where shocklets are observed. Therefore, a new

theoretical approach to vorticity transport using implications from these results will also be given which focuses on flow regimes where dominant modes exist.

Specifically, an experimental and theoretical study aimed at measuring and modeling the vorticity by using the laser induced fluorescence technique (LIF) is initiated. By using the energy balance equation and assuming that the process is isentropic the gas flow still can be considered as an ideal gas (The sample rate will be 500ns and the Reynolds number is as high as 10^8), the percentage of the nitrogen dioxide, which is the target for the laser beam and provides the fluorescence signal, is low enough so that reactive processes can be neglected. The density is measured by the calibration of the fluorescence against known densities. One can obtain the velocity and, with a time history the velocity fluctuations from the following

$$\frac{\rho_0}{\rho} = \left(1 + \frac{\gamma - 1}{\gamma} \mathbf{M}^2 \right)^{\frac{1}{\gamma - 1}} \tag{1}$$

where $\mathbf{M} = \dfrac{\mathbf{u}}{\mathbf{c}}$ is the Mach number

$$\mathbf{C}_p \frac{\partial \mathbf{T}}{\partial \mathbf{t}} + \left[\mathbf{C}_p \mathbf{T}_0 \left(\frac{1}{\rho_0} \right)^{\frac{\gamma - 1}{\gamma}} \frac{\gamma - 1}{\gamma} (\mathbf{P})^{\frac{-1}{\gamma}} - \frac{1}{\rho} \right] \mathbf{u}_i \frac{\partial \mathbf{P}}{\partial \mathbf{x}_i} = \frac{1}{\rho} \frac{\partial \mathbf{P}}{\partial \mathbf{t}} \tag{2}$$

The velocity profile across the shear layer provides a shear flow picture which will be used to understand the turbulent structure of the free shear layer. From the isentropy relation the pressure P, and the temperature T can be calculated when the density is measured. Therefore, all the data needed to investigate the behavior of the free shear layer are available and, consequently ,the vorticity signature can eventually be identified.

II . Background

To calculate the flowfield properties we need to use equations algebraic, differential, or integral which relate the pressure, the density, the temperature, the volume etc with boundary conditions connected to the problem of interest. The basic principles of mass conservation, Newton's law and energy conservation are applied to a small neighborhood surrounding a point in the flow resulting in differential equations which describe the flow properties at that point.

Basic equations in compressible flow

Continuity equation

This equation states that the net mass flow into the control volume must equal the rate of the increase of mass inside the control volume. It is the conservation of mass. The differential representation of this statement is

$$\frac{\partial \rho}{\partial t} + \text{div}\,(\rho V) = 0 \tag{3}$$

and the integral form of the same continuity equation is

$$-\oint_s \rho V.\, ds = \frac{\partial}{\partial t}\oint_v \rho dv \tag{4}$$

The momentum equation

The time rate of change of momentum of the fluid that is flowing through the control volume at any instant is equal to the net force exerted on the fluid

inside the volume. The differential representations of the momentum equation in the x, y ,and z directions respectively are

$$\frac{\partial(\rho V)}{\partial t} + \text{div}\,(\rho u V) = -\frac{\partial p}{\partial x} + \rho f_x$$

$$\frac{\partial(\rho V)}{\partial t} + \text{div}\,(\rho v V) = -\frac{\partial p}{\partial y} + \rho f_y$$

$$\frac{\partial(\rho V)}{\partial t} + \text{div}\,(\rho w V) = -\frac{\partial p}{\partial z} + \rho f_z \qquad (5)$$

where **f** is the body forces and **u, v, w** are the three components of the velocity **V** in a rectangular system of coordinates.

The integral form of that statement is

$$\oint_s (\rho V.ds)V + \oint_v \frac{\partial(\rho V)}{\partial t} dv = \oint_v \rho f dv - \oint_s p ds \qquad (6)$$

The energy equation

The differential form of the first law of thermodynamic is applied to an inviscid fluid flow and the result can be expressed as follows

$$\frac{\partial}{\partial t}(\rho(e + \frac{V^2}{2})) + \text{div}(\rho(e + \frac{V^2}{2})V) = -\text{div}(pV) + \rho\dot{q} + \rho(f.V) \qquad (7)$$

Where **e** is the internal energy of the element of fluid of interest and **q** is the heat added per unit mass. This equation is called the energy equation. The equations (4), (5), (6), (7) are the general equation which apply at any point in an unsteady three dimensional flow of compressible inviscid fluid. One can notice they are nonlinear partial differential equations.

The Reynolds equations of motion for incompressible flow

The above equations of motion are valid for the analysis of fluid flow turbulent or laminar. Let us consider an instantaneous velocity component at point as the follows[4], [5]

$$u(t) = \bar{u} + u'(t) \tag{8}$$

where

$$\bar{u} = \frac{1}{\tau}\int_{t-\tau/2}^{t+\tau/2} u(t)dt \tag{9}$$

and τ is the period of averaging and should include a large number of fluctuations.

For a quasi-incompressible flow , the mean values do not vary with time.

The equation of continuity of the instantaneous fluctuations is

$$\frac{\partial u'}{\partial x} + \frac{\partial v'}{\partial y} + \frac{\partial w'}{\partial z} = 0 \tag{10}$$

The Navier-Stockes equation for quasi-steady incompressible flows can be written as

$$\overline{a_x} = \bar{u}\frac{\partial \bar{u}}{\partial x} + \bar{v}\frac{\partial \bar{u}}{\partial y} + \bar{w}\frac{\partial \bar{u}}{\partial z} + \frac{\partial \overline{u'u'}}{\partial x} + \frac{\partial \overline{v'u'}}{\partial y} + \frac{\partial \overline{w'u'}}{\partial z} \qquad (11)$$

This equation is the equation of the mean flow for the x-direction. In the same way, equations can be written for the other directions. The quantities such as $-\rho\overline{u'u'}$ are the Reynolds stress components. Because of the presence of the unknown Reynolds stresses the solutions for the equation of the motion can not be found unless additional information about these stresses is available. Such information can be found using the mixing-length hypothesis for example.

Vorticity correlation and vorticity spectrum

The vorticity is the curl of the velocity with the components

$$\Omega_i(x) = \varepsilon_{ijk}\frac{\partial u_k(x)}{\partial x_j} \qquad (12)$$

Where ε_{ijk} is the alternating tenseur.

The vorticity vector is perpendicular to the velocity vector.

Let us consider the field shown in Fig.1

The vorticity correlations at points M and M' are given by the following expression

$$\langle \Omega_i(r_1)\Omega_j(r_1 + r)\rangle = \varepsilon_{ilm}\varepsilon_{jpq}\overline{\frac{\partial u_m(r_1)}{\partial x_l}\frac{\partial u_q(r_2)}{\partial x'_p}} \qquad (13)$$

where

$$x' = r_1 + r = r_2$$

Hence

$$\frac{\partial u_m(r_1)}{\partial x_l}\frac{\partial u_q(r_2)}{\partial x'_p} = \frac{\partial^2 R_{mq}(r)}{\partial r_l \partial r_p} \tag{14}$$

Therefore the vorticity correlations at points M and M' become

$$<\Omega_i(r)\Omega_j(r')> = -\delta_{ij}\nabla^2 R_{ll}(r) + \frac{\partial^2 R_{ll}(r)}{\partial r_i \partial r_j} + \nabla^2 R_{ij}(r) \tag{15}$$

From the continuity equation one obtains

$$R_{ij,j}(r) = R_{ij,i}(r) = 0 \tag{16}$$

Therefore

$$<\Omega_i(r)\ \Omega_j(r')> = -\nabla^2 R_{ij}(r) \tag{17}$$

If we take the Fourier transform of the vorticity correlations, we obtain

$$\bar{\omega}_{ij}(\tilde{k}) = (\delta_{ij}k^2 - k_i k_j)\phi_{ll}(\tilde{k}) - k^2\phi_{ji}(\tilde{k}) \tag{18}$$

where $\bar{\omega}_{ij}(\tilde{k})$ is called the vorticity spectrum tensor.

$$\bar{\omega}_{ii}(\tilde{k}) = k^2\phi_{ii}(\tilde{k}) \tag{19}$$

This last particular vorticity spectrum tensor is identical with the spectrum of viscous dissipation of kinetic energy.

Boundary approximations for the free turbulent shear flows

Free turbulent flows are bounded on at least one side by ambient fluid of nearly the same density which is not turbulent and is usually in irrotational flow[6]. From observation, it is found that the gradients of mean values in the direction of the main flow which is the ox direction are considerably less than in the transverse direction.

In addition to the boundary approximation in free turbulent shear flows the assumption of similarity or self-preservation will be made because the free turbulent shear layer region is extremely elongated in the main-flow direction. Self-preservation is used to indicate that the turbulence maintains its structure during the development of the turbulent region in the downstream direction of the main flow. The assumption of self-preservation allows one to reduce the number of independent variables and by this way the governing differential equations may be considerably simplified.

In free turbulent shear flow the production of turbulence is determined by the gradient of the mean-velocity distribution which depends on the turbulence generated upstream and transported downstream by turbulence diffusion by convection. Let us introduce L the length scale for variation of mean quantities which is the length scale in ox direction and l the transverse length scale that is in oy direction. The continuity equation for the mean flow can be written as

$$\frac{\partial U}{\partial x} + \frac{\partial V}{\partial y} + \frac{\partial W}{\partial z} = 0 \tag{20}$$

where U, V, W are the mean velocities in the three directions in the cartesian coordinates and u, v, w are the corresponding fluctuating velocities.

$U_s = U_{max} - U_{min}$ is the total variation of mean velocity over a transverse section of constant x. It follows that the transverse mean velocities are of order

$$(U_s + L\frac{dU_1}{dx})\frac{l}{L} \tag{21}$$

where U_1 is the flow velocity just outside the turbulent flow.

The momentum equation in the ox direction when the terms of order $\frac{l}{L}$ are omitted is

$$U\frac{\partial U}{\partial x} + V\frac{\partial U}{\partial y} + W\frac{\partial U}{\partial z} + \frac{\partial \overline{uv}}{\partial y} + \frac{\partial \overline{uw}}{\partial z} = U_1\frac{dU_1}{dx} + \nu\left(\frac{\partial^2 U}{\partial y^2} + \frac{\partial^2 U}{\partial z^2}\right) \tag{22}$$

Correspondingly, for the y direction one has

$$U\frac{\partial V}{\partial x} + V\frac{\partial V}{\partial y} + W\frac{\partial V}{\partial z} + \frac{\partial \overline{uv}}{\partial x} + \frac{\partial \overline{v^2}}{\partial y} + \frac{\partial \overline{vw}}{\partial z} = -\frac{\partial P}{\partial y} + \nu\nabla^2 V \tag{23}$$

For turbulent flow the Reynolds number is necessarily large and unless

$$(U_s + L^2\frac{d^2U_1}{dx^2})(U_s + U_1) \tag{24}$$

is comparable with $q_0^2L^2/l^2$, the equation is approximately

$$\frac{\partial \overline{v^2}}{\partial y} + \frac{\partial \overline{vw}}{\partial z} = -\frac{\partial P}{\partial y} \tag{25}$$

where q_0 is the scale velocity for the fluctuations and P_1 is the pressure just outside the free shear layer.

The ambient flow is irrotational and thus the equation of the motion for this part of the fluid is

$$\frac{dP_1}{dx} + U_1\frac{dU_1}{dx} = 0 \tag{26}$$

If oy is in the direction of maximum transverse gradient where the error in this approximation is smallest and $P + \overline{v^2} = P_1$, then the better approximation would be

$$U\frac{\partial U}{\partial x} + V\frac{\partial U}{\partial y} + W\frac{\partial U}{\partial z} + \frac{\partial \overline{uv}}{\partial y} + \frac{\partial \overline{uw}}{\partial z} + \frac{\partial(\overline{u^2} - \overline{v^2})}{\partial x} = U_1\frac{\partial U_1}{\partial x} \tag{27}$$

In this equation , the terms which are small when compared to the order $\frac{1}{L^2}$ have been neglected.

For flow homogeneous in the y direction with mean flow in the xoz plane the equation in the x component becomes

$$U\frac{\partial U}{\partial x} + W\frac{\partial U}{\partial z} + \frac{\partial \overline{uw}}{\partial z} + \frac{\partial(\overline{u^2} - \overline{w^2})}{\partial x} = U_1\frac{\partial U_1}{\partial x} \tag{28}$$

The equation of the energy is [7]

$$\rho\frac{DE}{Dt} = \frac{\partial}{\partial t}\rho E + \frac{\partial}{\partial x_j}(U_j \rho E) = \frac{\partial}{\partial x_j}\left(\kappa\frac{\partial T}{\partial x_j} + \sigma_{ji}U_i\right) \tag{29}$$

where E is the total energy and

$$\sigma_{ji} = -P\delta_{ij} + \mu\left(D_{ji} - \frac{2}{3}\theta\delta_{ij}\right) \tag{30}$$

Let us introduce the square of the velocity

$$U_i U_i = \overline{U}_i \overline{U}_i + 2\overline{U}_i u_i + u_i u_i$$
$$= \overline{U}_i \overline{U}_i + 2\overline{U}_i u_i + q^2$$

The rate of change of the kinetic energy is

$$\frac{\partial}{\partial t}\left(\frac{U_i U_i}{2}\right) = -\frac{\partial}{\partial x_j} U_j \left(\frac{P}{\rho} + \frac{U_i U_i}{2}\right) + \nu \frac{\partial}{\partial x_j} U_i \left(\frac{\partial U_i}{\partial x_j} + \frac{\partial U_j}{\partial x_i}\right)$$
$$-\nu\left(\frac{\partial U_i}{\partial x_j} + \frac{\partial U_j}{\partial x_i}\right)\frac{\partial U_i}{\partial x_j} \qquad (31)$$

Then the total rate of change of the turbulent kinetic energy reads

$$\frac{D}{Dt}\frac{q^2}{2} = -\frac{\partial}{\partial x_i}\overline{u_i\left(\frac{P}{\rho} + \frac{q^2}{2}\right)} - \overline{u_i u_j}\frac{\partial \overline{U}_j}{\partial x_i}$$
$$+\nu\frac{\partial}{\partial x_j} u_i\left(\frac{\partial u_i}{\partial x_j} + \frac{\partial u_j}{\partial x_i}\right) - \nu\overline{\left(\frac{\partial u_i}{\partial x_j} + \frac{\partial u_j}{\partial x_i}\right)\frac{\partial u_j}{\partial x_i}} \qquad (32)$$

In our experiment, the Reynolds number is to be high enough so that the viscous terms can be neglected compared to the others terms of this expression. Thus the total rate of change of the turbulent kinetic energy becomes

$$\frac{D}{Dt}\frac{q^2}{2} = -\frac{\partial}{\partial x_i}\overline{u_i\left(\frac{P}{\rho} + \frac{q^2}{2}\right)} - \overline{u_i u_j}\frac{\partial \overline{U}_j}{\partial x_i} \qquad (33)$$

Equation for the vorticity

The balance equation for mass, momentum and energy and the constitutive equation are the basic equations describing compressible flows.

The equation of continuity is

$$\frac{\partial \rho}{\partial t} + \frac{\partial}{\partial x_i} \rho U_i = 0 \tag{34}$$

The momentum equation is

$$\rho \frac{DU_i}{Dt} = -\frac{\partial P}{\partial x_i} + \mu \left[\frac{\partial^2 U_i}{\partial x_l \partial x_l} + \frac{1}{3} \frac{\partial}{\partial x_i} \theta \right] \tag{35}$$

where θ is the dilatation (the divergence of the velocity).

The equation for the momentum balance can be transformed to the one for the vorticity balance by taking the curl of equation (35)

This yields for the vorticity defined as $\Omega_k = \varepsilon_{ijk} \frac{\partial U_i}{\partial x_j}$ (36)

the equation

$$\rho \frac{D\Omega_k}{Dt} = \mu \frac{\partial^2 \Omega_k}{\partial x_l \partial x_l} + \frac{DU_i}{Dt} \varepsilon_{ijk} \frac{\partial \rho}{\partial x_j} + \rho \Omega_l \frac{\partial U_k}{\partial x_l} - \rho \Omega_k \theta \tag{37}$$

$$\begin{aligned} \frac{\partial U_i}{\partial x_j} &= \frac{1}{2}\left(\frac{\partial U_i}{\partial x_j} + \frac{\partial U_j}{\partial x_i} \right) + \frac{1}{2}\left(\frac{\partial U_i}{\partial x_j} - \frac{\partial U_j}{\partial x_i} \right) \\ &= \frac{1}{2} D_{ij} + \frac{1}{2} \Omega_k \varepsilon_{ijk} \end{aligned} \tag{38}$$

where ε_{ijk} is the alternating third-order tensor .

D_{ij} determines the deformation of the fluid and is called the deformation tensor. The antisymmetrical part $\Omega_k \varepsilon_{ijk}$ determines a rotation without deformation; it defines the vorticity of the motion.

Ω_k is called the vector of the antisymetrical tensor. It is identified with the vorticity and an equivalent relation is

$$\Omega_k = \varepsilon_{ijk} \frac{\partial U_i}{\partial x_j}$$

The significance of the first term on the right-hand side of equation (37) is readly seen through its mathematical similarity to the corresponding term in the Navier-Stokes equation. The action of viscosity produces diffusion of vorticity down a vorticity gradient, just as it produces diffusion of momentum down a momentum gradient.

The third term of th right -hand side of equation is the action of the variation of the velocity on the vorticity. In three dimensional flow there are vorticity-changing processes associated with that term.

The second and fourth terms on the right - hand side of equation (37) are due to the compressibility of the fluid, they are zero when the fluid is incompressible.

Shocks waves

The existence of shocks wave is one of the most distinguishing feature of compressible fluid motion. When both viscous and thermal diffusion are negligible for an ideal fluid (high Reynolds number and short measuring times) a shock wave is a discontinuity surface of flow field quantities such as the density, the pressure and the velocity component normal to the shock. For

the normal shock wave, the flow is supersonic on one side of the shock and subsonic on the other side. It is known that there is a strong relationship between vorticity and shock waves. The vorticity is created inside a curved shock wave through the interaction of fluid elements and the intensification of the compression in fluid elements.

In a situation where the pressure field is strong, the velocity difference between a local flow speed and a coherent structure's convective speed, will form a transient shock wave called a shocklet. The pressure field will always counter the initial structure circulation over a portion of the structure's contour and the formation of counter vorticity and consequent structure splitting will occur. The shocklets will affect the turbulence scale and production of counter fluctuating vorticity.

The flow parameters across the shock wave will be different. The jump conditions depend on the direction and the curvature of the shock wave.

The jump conditions relations are as follows [8] , [9] , [10] , [11]

$$\rho_2 = \frac{(\gamma + 1)M_s^2}{(\gamma - 1)M_s^2 + 2}\rho_1$$

$$P_2 = \frac{2gM_s^2 - (g - 1)}{(g + 1)}P_1 \qquad (39)$$

$$u_{n2} = \frac{(\gamma - 1)M_s^2 + 2}{(\gamma + 1)M_s^2}u_{n1}$$

$$u_{t2} = u_{t1}$$

where

$$M_s = \left(\frac{\rho|u|^2}{\gamma p}\cos\theta\right)^{1/2}$$

is the Mach number , and ρ_2 , p_2, u_{n2} , u_{l2} are the density, the pressure , the normal and parallel unit vectors to the shock wave respectively. With this, the spatial derivatives of the jump conditions can be obtained by taking the normal and tangential derivatives respectively

$$\frac{\partial \rho_2}{\partial l} = \frac{4(\gamma + 1)M_s^2\tan\theta}{r((\gamma - 1)M_s^2 + 2)^2}\rho_1$$

$$\frac{\partial P_2}{\partial l} = \frac{4\gamma M_s^2\tan\theta}{r(\gamma + 1)}P_1$$

$$\frac{\partial u_{l2}}{\partial l} = \frac{\left[(\gamma - 1)M_s^2 - 2\right]\tan\theta}{r(\gamma + 1)M_s^2}u_{n1} \qquad (40)$$

$$\frac{\partial u_{l2}}{\partial l} = -\frac{u_{n1}}{r}$$

$$\frac{\partial u_{l2}}{\partial l} = \left[\frac{2\left[(-\gamma+3)M_s^2 - (\gamma+5)\right]\tan\theta}{r(\gamma + 1)\left[(\gamma-1)M_s^2+2\right]}\right]u_{n1}$$

The normal derivatives are

$$\frac{\partial \rho_2}{\partial n} = \left[\frac{2M_s^2(1-M_s^2)+(\gamma+1)\left[3(\gamma-1)M_s^4-(\gamma-3)M_s^2+2(\gamma+2)\right]\tan^2\theta}{r(M_s^2-1)\left[(\gamma-1)M_s^2+2\right]^2} \right] \rho_1 \tag{41}$$

The same manipulations will be done to derive the other normal derivatives.

$$\frac{\partial u_{n2}}{\partial n} = \frac{2}{r(\gamma+1)} \left[\frac{2\gamma M_s^2-(\gamma-1)}{(\gamma+1)M_s^2} - \frac{3M_s^2+1}{M_s^2-1}\tan^2\theta \right] u_{n1}$$

where the radius of the curvature is

$$r = -\frac{1}{\frac{\partial \theta}{\partial l}}$$

and θ is the angle of attack.

Thus, the vorticity generated behind the shock wave can be computed from the jump conditions and the spatial derivatives of the velocity as follows

$$\omega_2 = \frac{\partial u_{l2}}{\partial n} + \frac{u_{l2}}{r} - \frac{\partial u_{n2}}{\partial l} \tag{42}$$

that is

$$\omega_2 = \frac{4(M_s^2-1)^2 \sin\theta}{r(\gamma+1)M_s^2((\gamma-1)M_s^2+2)^2} |u| \tag{43}$$

Eddy shocklets

The existence of eddy shocklets in compressible turbulence has important consequences leading for example to conversion of turbulent kinetic energy to internal energy via the pressure-dilatation correlation and additional kinetic energy decay through dilatational dissipation produced by shocklets [12]. Most of the studies of turbulent structures have been done on low Mach number flows where the compressibility does not play an important role and in this case it is impossible to form weak shock wave.

In both 2D and 3D simulations, at sufficient high Mach numbers, eddy shocklets are found and are confirmed to display the characteristic of an oblique shock wave[13]. However, in the 3D simulations these shocks are weak.

Shocklets and vorticity generation

For supersonic flows, regions of strong compression can be formed resulting in the formation of shock wave in the flow. The propagation of such shock wave or eddy shocklet will interact with the flow field and other structures [14] in supersonic shear flow. The shocklets affect the structure's size and transfer turbulent energy in the flow field and produce vorticity behind the shocklets. The turbulent shocklets are associated with bursting phenomenon in the supersonic free shear layer. The bursts are in turn associated with the evolution of structure and the transfer of turbulent energy in the flow field. First evidence of this bursting phenomena was provided by Zhang et al. as shown in Fig. 2 where the free shear layer shows concentrated collections of strong density signals.

Lee et al .[15] have found that shocklets can be formed in three dimensional homogeneous turbulence simulations. They concluded that the presence of shocklets is important due to the conversion of turbulent kinetic energy to internal energy via the pressure dilatation correlation.

Kolmogorov length

An essential characteristic of fully turbulent fluid is the presence of vorticity in large amounts and the development of vorticity in irrotational fluid depends, in the first place on viscous diffusion of vorticity across the bounding surface.

A qualitative description of the transfer of vorticity to the irrotational fluid may be given by considering the influence on the viscous diffusion of eddies in groups of increasing size[16]. The smallest eddies would produce ripples on an initially sharp interface with wavelengths comparable with the Kolmogorov length

$$l_s = \left(\frac{\nu^3}{\varepsilon}\right)^{1/4} \tag{44}$$

and induce rates of strain of order $\beta = \left(\frac{\varepsilon}{\nu}\right)^{\frac{1}{2}}$ which compress the diffused layer at the wave crests and strectch it in the throughs.

After a time t, the average advance of vorticity into the ambient fluid will be roughly

$$\left(\frac{\nu}{\beta}\left(e^{2\beta t}-1\right)\right)^{1/2} = l_s e^{\beta t} \tag{45}$$

where β is the entrainment parameter defined as

$$\beta = \frac{U+\frac{1}{2}u}{|u|}\frac{dl_0}{dx} \tag{46}$$

which is a constant for any kind of self-preserving flow but varies considerably from one kind to another.

The area Mach number relation at the outlet of the nozzle in the Ludwieg tube during the measuring time

One can find in the litterature the way to derive the Reynolds number at the outlet of the nozzle. The higher pressure is P_4 and P_0 the stagnation pressure and $T_a = T_0 = T_4$ the stagnation temperature where T_4 is the temperature of the room. Let us first of all derive the normal shock wave relation

The basic normal shock wave relations (respectively the continuity, the momentum and the energy equations) are

$$\begin{aligned} \rho_1 U_1 &= \rho_2 U_2 \\ p_1 + \rho_1 U_1 &= p_2 + \rho_2 U_2 \\ h_1 + \frac{U_1^2}{2} &= h_2 + \frac{U_2^2}{2} \end{aligned} \qquad (47)$$

All the parameters ahead of the shock wave have subscript 1 and those behind the shock wave have 2.

By combining the continuity equation , the momentum equation ,the equation of energy and the speed of sound in a calorically perfect gas we obtain the following relation[9], [18]

$$a^{*2} = U_1 U_2 \qquad (48)$$

This relation is called the Prandtl relation where a^* is the speed of sound when we suppose that the Mach number is 1 .

A relation between the Mach number ahead and behind the shock wave can also be derived from the Prandtl equation

A relation between the Mach number ahead and behind the shock wave can also be derived from the Prandtl equation

$$1 = \frac{U_1}{a^*}\frac{U_2}{a^*} = M_1^* M_2^* \tag{49}$$

or

$$M_2^* = \frac{1}{M_1^*} \tag{50}$$

The Mach number behind the shock wave is

$$M_2^2 = \frac{1 + [(\gamma - 1)/2]M_1^2}{\gamma M_1^2 - (\gamma - 1)/2} \tag{51}$$

The flow ahead the shock wave must be supersonic hence this last relation shows that the flow behind the shock wave must be subsonic.

The shock relations for the other parameters are

For the pressure

$$\frac{P_2}{P_1} = \frac{1 + \gamma M_1^2}{1 + \gamma M_2^2} \tag{52}$$

For the temperature

$$\frac{T_2}{T_1} = \left[\frac{1 + \gamma M_1^2}{1 + \gamma M_2^2}\right]^2 \left(\frac{M_2}{M_1}\right)^2 \tag{53}$$

And for the density one obtains

$$\frac{\rho_2}{\rho_1} = \left[\frac{1 + \gamma M_2^2}{1 + \gamma M_1^2}\right]\left(\frac{M_1}{M_2}\right)^2 \tag{54}$$

Finally the stagnation magnitude of the parameters can also be obtained.
If the area at the throat of the the nozzle is A^* and that at the outlet is

A_{outlet}, hten the continuity equation between the two locations is

$$\rho^{*} U^{*} A^{*} = \rho U A_{outlet} \tag{55}$$

I lence the ratio of A^{*} to A_{outlet} is

$$\frac{A_{outlet}}{A^{*}} = \frac{\rho^{*} U^{*}}{\rho U} \tag{56}$$

or

$$\frac{A^{*}}{A_{outlet}} = \frac{M}{\left[\frac{2}{\gamma + 1}\left(1 + \frac{\gamma - 1}{2} M^{2}\right)\right]^{\frac{\gamma + 1}{2(\gamma - 1)}}} \tag{57}$$

is the ratio of the areas of the throat and the outlet. This equation shows us that the Mach number at any location in the Ludwieg tube is a function of the ratio of the local tube area to the sonic throat area. From this, the Reynolds number at the outlet of the nozzle of the Ludwieg tube during the measuring time can be found since generally the following relation holds

$$\frac{R_e}{D} = (P_4, T_0, M) \tag{58}$$

and $$M = M(A^{*}/A_{outlet}) \tag{59}$$

Distinguishing the three states of flow at the nozzle's exit

When the diaphragm breaks, one can deal with three types of flow states.

1- There can exist a wake and an expansion wave from the nozzle. This means that the back pressure around the outlet of the nozzle is less than the pressure of the flow at the outlet section. Then the Mach number of the flow behind the expansion wave will be more than the Mach number of the initial flow at the outlet. The directions of the axis of the wake and the flow behind the expansion wave are different from the direction of the initial flow.

2- There may be a wake and an oblique shock wave from the outlet of the nozzle. This means that the back pressure is more than the pressure of the flow at the outlet. In this case ,the Mach number behind the shock wave will be less than the Mach mumber of the initial flow. The direction of the axis of the wake and the flow behind the shock wave are inward more or less aimed toward the center of the test section.

3- There may be neither expansion waves nor shock waves from the outlet of the nozzle, just a wake in the form of a free shear layer. This state means that the back pressure around the oultet of the nozzle is the same as the pressure of the flow at the outlet. In this case, the Mach mumber,Reynolds number and the direction of the initial flow are unchanged and the direction of the axis of the wake will be the same as that of the initial flow. This is the state that we need and have created in our experiment on the turbulent compressible flow. The pressure conditions (that is, a determination of P_4 and the ratio P_4/P_1)for this are determined by studies of shadographs photographs at the test section and are confirmed by the density measurements during the Ludwieg tube firings.

The velocity calculation

In our experiment a supersonic flow is generated by the Ludwieg tube in which velocities and velocity gradients can be determined. The previous discussions make clear the important role which such determinations play in

our ability to understand turbulent flow. The sample rate is 500 ns and the Reynolds number is as high as 10^8 . In this case the process can be considered isentropic. In addition, the gas of the flow (2% of NO_2 and 98 % of N_2 mixture) can be considered as an ideal gas since the percentage of NO_2 is small. Then the following energy balance equation holds

$$h_1 + \frac{1}{2} u_1^2 = h_2 + \frac{1}{2} u_2^2 \tag{60}$$

In our case this equation can be written as

$$C_p T + \frac{1}{2} u^2 = C_p T_0 \tag{61}$$

The index 0 stands for frozen value. The speed of the sound is

$$a^2 = (\frac{\partial p}{\partial \rho})_s = \gamma RT \tag{62}$$

and it enables us to write the energy equation as follows

$$\frac{1}{2} u^2 + \frac{a^2}{\gamma - 1} = \frac{a_0^2}{\gamma - 1} \tag{63}$$

This last equation can be written in a way such that the Mach number and the density are involved that is

$$\frac{\rho_0}{\rho} = (1 + \frac{\gamma - 1}{2} M^2)^{\frac{1}{\gamma - 1}} \tag{64}$$

The free stream velocity can be calculated when the density is obtained from the measurement using the calibration curves.

Another assumption can be made if the Reynolds number is high enough and the measuring time is short. In this event the flow can be considered inviscid and non conducting. The energy equation is

$$\rho f_i u_i + \rho q - \frac{\partial}{\partial t}(Pu_i) = \frac{\partial}{\partial t}(W) + \frac{\partial}{\partial x_j}(Wu_j) \tag{65}$$

Where

$$W = \rho e + \frac{1}{2}\rho u^2 \tag{66}$$

and f_i is an external force per unit mass.

Therefore

$$\rho \frac{D}{Dt}\left(\frac{1}{2}u^2\right) = - u_i \frac{\partial P}{\partial x_i} + \rho f_i u_i \tag{67}$$

and

$$\frac{De}{Dt} + p\frac{D(1/\rho)}{Dt} = q \tag{68}$$

The total enthalpy is

$$\frac{D}{Dt}\left(h + \frac{1}{2}u^2\right) = q + f_i u_i + \frac{1}{\rho}\frac{\partial P}{\partial t} \tag{69}$$

And for an ideal gas

$$h + \frac{1}{2}u^2 = C_p T + \frac{1}{2}u^2 \tag{70}$$

When there is no external force the first term on the left side in equation (65) is zero. The first term in the right-hand side of equation (69) is also zero when the flow is nonconducting .

From the well known relation

$$\frac{P}{P_0} = \left(\frac{\rho}{\rho_0}\right)^{\gamma} = \left(\frac{T}{T_0}\right)^{\frac{\gamma}{\gamma - 1}} \tag{71}$$

one can obtain the following equation

$$C_p \frac{\partial T}{\partial t} + \left[C_p T_0 \left(\frac{1}{\rho_0} \right)^{\frac{\gamma-1}{\gamma}} \frac{\gamma - 1}{\gamma} (P)^{\frac{-1}{\gamma}} - \frac{1}{\rho} \right] u_i \frac{\partial P}{\partial x_i} = \frac{1}{\rho} \frac{\partial P}{\partial t} \tag{72}$$

From the isentropy relation the pressure and the temperature can be calculated when the density is measured. The local density histories are obtained and also the time and space derivatives of the density, the pressure and temperature can be calculated from the quantities which have been measured. Therefore the x component of the Navier-Stokes equation in inviscid and nonconducting flow is

$$\frac{\partial U}{\partial t} + U\frac{\partial U}{\partial x} + V\frac{\partial U}{\partial y} + W\frac{\partial U}{\partial z} = -\frac{1}{\rho}\frac{\partial P}{\partial x} \tag{73}$$

From the three equations (71, 72, 73) the three components of the velocity can be obtained. The flow in the free shear layer is predominantly two-dimensional. The streamwise and transverse components of the velocity are then calculated.

From our experiment results, the derivatives of the velocity can be obtained. We will use the technique similar to the finite - difference grid as follows

The computational fluid dynamic techniques are predicated on the ability to expand the flow field proprieties in terms of a Taylor's series [19].

If $u_{i,j}$ is the x component of the velocity at point (i, j) then the velocity $u_{i+1,\,j}$ at point (i+ 1 , j) can be obtained from

$$u_{i+1,\,j} \approx u_{i,j} + \left(\frac{\partial u}{\partial x}\right)_{i,j} \Delta x \tag{74}$$

The higher order terms have been neglected. The same thing can be done in the y direction between $u_{i\,,\,j+1}$ and $u_{i\,,j}$ to obtain

$$u_{i\,,\,j+1} \approx u_{i\,,j} + \left(\frac{\partial u}{\partial y}\right)_{i,j} \Delta y \tag{75}$$

The approximation used to get the derivative of the velocity in x and y direction is good if Δx and Δy are small enough. In our experiment $\Delta x = \Delta y = 0.5$ mm.

That is a good resolution which ensures us of a good approximation. It has been possible to have that resolution because the optical set up (system II) is resting on an optical table which has hydraulic legs so that the vibrations in the room are absorbed.

The flow in the free shear layer is predominantly two-dimensional. The streamwise and transverse components of the velocity are then calculated.

III. Experimental set-up

The Ludwieg tube

The type of wind tunnel in which the experiments have been performed is the Ludwieg tube. It is a conventional shock tube modified by the insertion of a layer-spilling asymetric supersonic nozzle into the section upstream from the diaphragm. When the diaphragm breaks, an expansion wave moves upstream into the high-pressure section through the nozzle causing the local pressure, density, and gas velocity to change with time and as a function of distance from the location of the diaphragm. At a time determined by the ratio of the nozzle's throat area to its exit area, the nozzle is choked, that is, the mass flow rate is frozen, and stable steady supersonic flow is established in the exit region. The duration of this steady period is determined by the round trip time for the head of the expansion wave to travel from the throat of the nozzle to the upstream termination of the high-pressure section. When the diaphragm breaks, other wave phenomena are also produced; viz, a shock wave and a contact surface travel downstream into the low pressure section. One can find derivation of the formulas relating the nozzle's parameters to the initial conditions of the tube. By this way, high Reynolds numbers can be maintained in the exit region under conditions of steady supersonic flow[17]. The x-t diagram and a schematic of the Ludwieg tube are shown in Fig.3. A photograph of the Ludwieg tube is shown in Fig. 4.

The Ludwieg tube has two parts : a 6-in. diameter, 5-ft long cylindrical end piece and a 3-ft long transition piece that changes from 6-in diameter circular cross section to a 3.6 -x 3.6-in. square at the diaphragm. The transition piece has

a plunger for rupturing the diaphragm. The high pressure section has five parts: a 6-ft -long ,3.6-x3.6-in. square test section with five optical ports on each face and corresponding pressure ports; a 3-ft -long transition piece for the change from a 3.6-x 3.6-in. cross section to the 6-in.-diameter circle; a 5-ft-long,6-in.- diameter cylindrical piece; and two pieces that are each quarter-circle arcs of 2-ft radius with 6-in. diameter cross sections. The curved sections conveniently extend the overall length of the period of steady supersonic flow. The wall thickness is roughly of order of 0.3 inch.

A diaphragm is placed into the tube to separate the low pressure side from the high pressure side and a vaccum pump will pump down the low pressure section down to 110 torr. On the high pressure side, a pure Nitrogen dioxide is loaded up to 33.5 torr slowly to prevent NO_2 condensation. Next we add pure nitrogen to NO_2 up to about 1675 torr (absolue). One must run several times in order to control the flatness of the free shear layer which is very sensitive to the ratio of the high pressure P_4 to the low pressure P_0.

Once the pressures read the right magnitude and there is no leak in the system, we make sure the trigger system is armed properly and also the anolog-digital converters are armed properly (with the required sweep time and delay time). Then the diaphragm is ruptured and the data are collected. Since the nitrogen dioxide is poisonous and heavier than the air, extreme care must be taken in manipulating it. After firing the tube, it must be purged carefully for a long period of time before another run. The system is purged by pumping down the tube and by loading pure nitrogen in it for a while.

The anolog-digital converters are triggered by a piezo-electric transducer located upstream of the diaphragm. In a piezo-electric transducer, the application of a directed compression to a quartz or similar cristal causes an electric charge to appear accros its faces. This effect is called the piezo-electric effect [10]. Actually

in our system there are two transducers , they enable us to monitor the expansion fan, to determine the delay time for the trigger system and to compute the drop in the pressure in the high pressure side and consequently the drop in the temperature can be calculated. In our experiment the delay time was 14 ms.

Optical set-up

An optical system is used to collect the fluorescence signals from the test section. (See Fig. 5.) An argon laser provides a beam which is split in three beams such that the cross section of the set of the beams is in triangular form. The beams are sent through the free shear layer. The intensity of the fluorescence emitted by NO_2 molecules depends on the density of the NO_2 molecules in the flow and the intensity of incident laser beam. When the diaphragm which separates the high pressure side from the low pressure side is ruptured, an expansion wave moves upstream into the high pressure section. The expansion wave causes the local pressure, density, and velocity to change with time. The intensity signals collected by the photomultiplier tubes represent the local density of NO_2 molecules which is mixed with N_2 as the flow gas. Therefore , the density or density fluctuation of NO_2 represent the flow density or density fluctuation. After the diaphragm is ruptured , there is a time at which flow through the nozzle is chocked, as a result of conservation of mass, the flow rate is frozen and stable, and steady supersonic flow is established in the exit region of the nozzle. A free shear layer is created on the nondiverging side of the nozzle as suggested by Fig. 6 where the typical measuring stations are also indicated. By design, as a result of the dimensions of the system, tube wall does not affect the shear layer since the step of the nozzle is large compared to the size of the shear layer. The Mach number is 2.02

for all of the measurements reported here. (This is a consequence of the specific nozzle chosen; it can be changed for future experiments by a different choice of nozzles.)

The optical set-up consists of two systems which are labeled as system I and system II. A laser beam from an argon ion laser 488.0 nm wave length is used as the overall light source.

System I provides as output three beams in triangular form. Mirrors and lenses are aligned in a way such that a large beam is produced and a mask with three holes is placed in the path of the beam. The three beams formed in this way have the same size and the same intensity. They are 0.8 cm apart in the first phase and another set of lenses translates the three beams so that they are much closer to each other, 1.0 mm apart. This distance provides good spatial resolution so that an approximation can be made which allows the calculation of velocities from the density measurements.

Since the points where the measurements will be made are so close, it is not possible to collect data using optical data using optical fibers unless a magnified image is produced. This is the function of system II. It consists of lenses and mirrors which magnify the distance between the beams from 0.5mm to 1 cm. At the image plane of the magnified free shear layer, fiber optic light pipes are arranged to collect the fluorescent signals which are carried to the individual photomultipliers. These outputs are subsequently transmitted to the anolog to digital converters for ultimate storage, through software and hardware interfaces on computer disks. The spatial resolution of the measurement mainly depends on the separation between the measuring points. The measuring points are arranged such that the velocity components can be obtained and therefore one component of the vorticity can be computed.

Density calibration

In this experiment the NO_2 molecules which are mixed with pure N_2 molecules (2% of N_2 in 98% of NO_2) provide a good target for resonance radiation after excitation with the incident laser beam at 488.0 nm wave length. The NO_2 molecules are pumped up to vibrational excitation states by the argon ion laser. Although the NO_2 spectrum extends from 800 nm to near 400 nm with a very high density of lines, the fluorescence induced by the chosen laser line (which is in the blue) is in the yellow and quite distinguishable for the excitation with simple filtering. The intensity of the fluorescence emitted by NO_2 molecules is related to the density of the NO_2molecules in the flow and to the intensity of the incident laser beam. This signal represents the local density of NO_2 molecules and therefore the density and the density fluctuation of NO_2 represent the density fluctuation of the flow.

The relation between the density and the intensity of the fluorescence is called the calibration relation. For the chosen mixture mentioned earlier, the intensity of the fluorescence is a function of the density and decays exponentially as the density of NO_2 increases. This can be explained by the interaction between the NO_2 molecules when an excited molecule of NO_2 interacts with another NO_2 before falling back to a lower energy level radiates fluorescence light can transfer energy to another molecule. Therefore the higher concentration of NO_2molecules the larger the number of interactions of NO_2 molecules which results in a decreasing fluorescence. For a different percentage of NO_2 the calibration is shifted but the functional relation between the intensity and the density is unchanged.

The effect of temperature on the calibration has been determined. The set-up is shown in Fig. 7; a controlled concentration of NO_2 in mixture with N_2 is temperature controlled by a bath of dry ice (CO_2). The relation between density

and fluorescence is determined over a range of temperatures. From these measurements, the temperature calibration factor is calculated using a least squared fit to the appropriate density of states multiplicative factor. A sample of these results is shown in Fig. 8. In Fig. 9 the correctness of the use of a multiplicative factor is tested for a sample of data collected for a range of temperatures; the overall exponential behavior for the temperature-independent part of the density-fluorescence calibration is confirmed. Since the actual flow speed in the free stream is known as well as the flow speed at the axis (from previous measurements), the calibration factor is easily checked. The temperature reached in the free stream is computed from the expansion wave measurements of pressure at the Ludwieg tube's walls by the two transducers located upstream of the lip of the nozzle. The temperature is found to be roughly T= 274 °K for the temperature reached when the supersonic flow is constant in the Ludwieg tube.

IV- Analytical procedure, results, and discussions

Second viscosity

It is well known that the second (or bulk) viscosity and the chemical relaxation time are implicitly connected. However it is only relevant in processes where there is a compression or an expansion and it is usually regarded as small even when it is relevant. Nonetheless, it now seems appropriate to determine in general whether or not there can be circumstances where the influence of second viscosity might be important. This is the situation where the velocity gradient is important. In the appendix, one can find an apprroach that uses the macroscopic entropy production rate equation in a reactive flow in order to explore the possibility of an explicit connection between the second viscosity and the relaxation time.

Vorticity calculation

In a given flow field, it is possible that some parts of the flow field are irrotational, while other parts are not. The rotation of a fluid element shall be denoted by the rotation vector which is defined as the average angular velocity of two originally perpendicular lines conceptually attached to the fluid element of interest [20]. It is customary to deal with the vorticity vector Ω which is defined as

$$\Omega = 2\,\omega \tag{76}$$

The kinematic properties of the vorticity are similar to those of the velocity vector. The components of the vorticity vector in the cartesian coordinates are as follows

$$\Omega_x = \frac{\partial w}{\partial y} - \frac{\partial v}{\partial z}$$
$$\Omega_y = \frac{\partial u}{\partial z} - \frac{\partial w}{\partial x} \qquad (77)$$
$$\Omega_z = \frac{\partial v}{\partial x} - \frac{\partial u}{\partial y}$$

Where u, v and w are the velocity components in the x, y and z directions respectively .

In any coordinates system, the vorticity vector satisfies the corresponding incompressible vorticity continuity equation

$$\int_s (n.\Omega)\, ds = 0 \qquad (78)$$

s is the closed surface enclosing an arbitrary volume of fluid of interest and **n** the unit outward normal to the surface element **ds**. The kinematic property of the vorticity is referred to as the conservation of vorticity.

Let us introduce the circulation Γ of the vorticity

$$\Gamma = \int_s (n.\Omega)\, ds \qquad (79)$$

For a given vortex tube in an incompressible flow, the circulation of the vorticity is constant and is essentially the product of the mean vorticity and the cross-sectional area. Therefore when the cross-sectional area is smaller, the vorticity is stronger. That is why in a tornado which is a giant vortex tube the air particules in the center rotate with a much higher angular velocity near the ground where the funnel is narrowest [4]. The vorticity field of a compressible

flow satisfies $\mathrm{div}\Omega = 0$ even though the divergence of the velocity is no longer zero.

Let us also consider, for example, a finite thin flat wing which is undergoing lift. The fluid beneath the wing near the wing tips will tend to spill over the tip, then the circulation of the vorticity will be non-zero. Therefore there must be vorticity in the fluid . The vortex tube cannot end in the fluid, but must attach itself to the solid body (as a tornado attached to the ground) or extend to infinity. Consequently, when the lift is present ,the flow field cannot be completely free from vorticity. Then a drag force must be experienced by the wing. A non zero drag force called induced drag must always be present when there is lift. Conversely in the absence of the vorticity the net lift experienced by a finite body in steady flow is also zero. The vorticity is then an important topic in fluid mechanics.

The compressibility is expressed mathematically through the divergence of the fluid velocity and it is responsible for the effects such as sound waves and shock waves. The vorticity on the other hand, is expressed mathematically through the curl or rotation of the fluid velocity and it is primarly responsible for convective mixing and turbulence[21]. By making use of the isentropic relation the pressure, and the temperature can be calculated. In our experiment we are interested in measuring one component of the vorticity. Since the multipoint measurements are set such that 3- dimensional local density histories are obtained in our data, the time and space derivatives of the density, pressure and temperature can be calculated.

Data and results

The technique consists of measuring the density fluctuation by using the fluorescence emitted by a mixture of 2% of NO_2 and 98% of N_2 targeted by a

laser beam split in three beams of the same size. Seven measuring points are selected in a certain way such that a velocity calculation can be made in the free shear layer at the exit of the supersonic nozzle in the Ludwieg tube. The calibration curves (fluorescence vs density plots) have been used to obtain the density fluctuation. The analog-digital converters used are the NICOLET 400 series and the photomultipliers are HAMAMATSU phototubes. The pressure has been controlled by a digital MKS Baratron which provides the reading of the low and high pressures. A sample of on-axis fluorescence voltage signatures is given in fig. 10. The raw data measurements show the appropriate qualitative trend with increasing distance from the nozzle's edge.

Similarly for fully calibrated results, the trends along the axis and transverse to the axis are correct. This conclusion is based on surveys throughout the free shear layer, below as well as above the axis. A sample of these measurements is given in fig.11. As described below, the density measurements obtained from the calibrated fluorescence signals provide the input for the velocity computations which give us the vorticity data we require.

The density fluctuations we have obtained in our facilities are in good agreement with the behavior of the gradient of the density which must decrease from the lower edge to the upper edge of the free shear layer. In this technique of LIF, more than the seven probes (a large number of points from which the fluorescence will be collected) would have been required in order to measure all three components of the vorticity; that is why we have limited ourselves to preparing for the measurement of one component of the vorticity.

If the measurements are not made in the free shear layer when it is flat, this expected relationship between the gradient of the density and the location

of the point from where the fluorescence is being collecting will not be observed. This test enables us to make certain that the measurements are good.

In free turbulent shear flow , there is production of turbulence. But this production is determined by the gradient of the mean velocity distribution, which depends in turn on the turbulence diffusion and by convection. This close connection between the turbulence and the mean- velocity distribution at any section and those upstream makes it reasonable to expect similarity of the total pattern even though turbulence is continuously being produced by the main motion through the turbulence shear stresses. However the flow requires some distance downstream before the self preserving condition is reached. From previous measurements, we are able to focus on the region in the flow where the self preserving status has been acquired.

Since the relationships are known with which velocities can be determined from density [11], it remains to show that evidence of sharp velocity gradients can be found in the velocity histories. Such gradients are clearly present if signatures of velocity driven bursts in time are found analogous to density bursts already observed in the free shear layer and associated with the production of turbulent shocklets (Johnson et al . 1994). The results from such studies are illustrated in Figs. 12, 13, and 14.

A sample of an axial velocity history is given in Fig. 12 with the corresponding transverse velocity history given in Fig. 13. These are Ux and Uy, two components of the local flow velocity U. Although our set-up affords an estimte of Uz, the third component, the spectral analysis of it shows a noise-like behavior and the standard signatures of turbulence were not observed. Nonetheless, with our set-up a reliable set of velocity calculations has been produced which are adequate for one component of vorticity.

For Ux and Uy, velocity fluctuations are observed as follows :

$$u'_i = u_i - \langle u_i \rangle \tag{80}$$

where $\langle u_i \rangle$ is the average value of u_i

From this, we determine the history of $\rho u'_x u'_y$ as shown in fig. 15. The evidence of bursts in $\rho u'_x u'_y$ is quite clear. It provides a strong basis for an expectation of dramatic influence from changes in U on the turbulent behavior.

A model for one component of the vorticity in the free shear layer

In our experiment, we have developed the ability to measure one component of the vorticity at the same location in the free shear layer of a supersonic flow. By using the free shear layer approximations we have already used to derive the equation of the motion, we can derive the equation for the vorticity as follows

$$\rho \frac{D\Omega_k}{Dt} = \mu \frac{\partial^2 \Omega_k}{\partial x_l \partial x_l} \tag{81}$$

This equation has been derived from equation (37) in which all the terms are zero or are assumed to be negligible compared to the first term on the right side which is

$$\mu \frac{\partial^2 \Omega_k}{\partial x_l \partial x_l} \tag{82}$$

The second term in equation (37) is negligible because the derivative of the velocity with respect to x which is small is involved, the third term is zero because the divergence of the velocity multiplied by the vorticity components is also negligible for the third component of the vorticity.

By applying the boundary approximation to our case this term (82) becomes

$$\mu \frac{\partial^2 \Omega}{\partial y^2} \tag{83}$$

where Ω is the component of the vorticity in the z direction

Thus the vorticity equation becomes

$$\rho \frac{D\Omega}{Dt} = \mu \frac{\partial^2 \Omega}{\partial y^2} \tag{84}$$

or if we take into account the following relation (the euleurian derivative of the vorticity)

$$\frac{D\Omega}{Dt} = \frac{\partial \Omega}{\partial t} + U \frac{\partial \Omega}{\partial x} + V \frac{\partial \Omega}{\partial y} + W \frac{\partial \Omega}{\partial z} \tag{85}$$

The last three terms in the left hand side in relation (85) are negligible using the boundary layer-like approximations. Thus the equation for the vorticity can be written as

$$\frac{\partial \Omega}{\partial t} - \frac{\mu}{\rho} \frac{\partial^2 \Omega}{\partial y^2} = 0 \tag{86}$$

This equation is a partial differential equation of the type of one - dimensional heat equation.

From all of these derivations,we can now express the turbulent vorticity Ω' in term of the derivative of the fluctuating part of the velocity with regard to our approximations as

$$\Omega' = - \frac{\partial u'}{\partial y} \tag{87}$$

We can at this stage write the relation which enables us to analyse the behavior of the transverse component of the vorticity.

The equation for the vorticity becomes a differential equation of a special type. Because we are dealing with one component of the vorticity which can be expressed as a scalar , that component can in turn be treated as a scalar. The differential equation that governs the evolution of the vorticity in the free shear layer at a fixed point and in a region where there is no intermittency (since the measurements have been made at a fixed point on the x axis in a region which is far away from the boundary of the free shear layer) can be expressed in term of the fluctuation part of the velocity.

For small disturbances the fluctuation part of the vorticity at a fixed point along the x axis can be written as

$$\Omega' = \Omega'_0 \exp i(\omega t - ky) \tag{88}$$

where ω is the angular velocity.

Equation (86) becomes for Ω'

$$i\omega + \nu k^2 = 0 \tag{89}$$

where

$$\nu = \frac{\mu}{\rho}$$

Let us assume that ω is constant, real and positive; then k would be a complex quantity with two values

$$k = \sqrt{-i\frac{\omega}{\nu}} \tag{90}$$

ie

$$k_1 = \sqrt{\frac{\omega}{2\nu}}\,(1-i) \tag{91}$$

or

$$k_2 = -\sqrt{\frac{\omega}{2\nu}}\,(1-i) \tag{92}$$

The vorticity fluctuation can be written as

$$\Omega'_1 = \Omega'_0 \exp\left(\sqrt{\frac{\omega}{2\nu}}\,y\right) \exp i\left(\omega t + \sqrt{\frac{\omega}{2\nu}}\,y\right) \tag{93}$$

or

$$\Omega'_2 = \Omega'_0 \exp\left(-\sqrt{\frac{\omega}{2\nu}}\,y\right) \exp i\left(\omega t - \sqrt{\frac{\omega}{2\nu}}\,y\right) \tag{94}$$

One of these solutions is not consistent with regard to the behavior of the vorticity. From the x axis to the upper edge of the free shear layer, the vorticity which can be expressed as the derivative of the velocity with respect to the y coordinate, decreases. Actually both solutions represent the evolution of the vorticity in the negative y for (93) and in the positive y for (94).

Thus, the amplitude of the vorticity must decrease as y increases otherwise the main flow would not be irrotational as it should be. Hence we must retain the solution Ω_2 since we are measuring the vorticity in the area where y is positive.

In addition to this, since the measurements are taken at the axis of the free shear layer, y can be considered zero. Thus, we obtain for the fluctuating part of the vorticity the following expression

$$\Omega'(t) = \Omega'_0 \exp i\omega t \tag{95}$$

This expression will be written for clarty as follows

$$\Omega'(t) = A_0 \exp i\omega t \tag{96}$$

Let us take the Fourier transform of the above expression by writting first of all the following Fourier series

$$\Omega'(t) = \sum_{n=-\infty}^{\infty} A_n \exp in\omega_0 t \tag{97}$$

Let us now consider the Fourier transform[25]

$$\Omega'(t) = \int A(\omega) \exp (i\omega t) d(\omega) \tag{98}$$

where

$$A(\omega) = \frac{1}{2\pi} \int_{-} \Omega'(t) \exp (- i\omega t) dt \tag{99}$$

The power spectrum is

$$S(\omega) = \left|A(\omega)\right|^2 \tag{100}$$

In our case the process begins at a time t = 0 such that

$$\Omega'(t) = \Omega'_{0} \exp (i\omega_{0}t) \qquad \text{for } 0 < t < \infty \tag{101}$$

$$\Omega'(t) = 0 \qquad \text{for } t < 0$$

Thus the calculation of $A(\omega)$ leads to

$$A(\omega) = \frac{\Omega'_{0}}{2\pi i(\omega - \omega_{0})} \tag{102}$$

And the power spectrum is

$$S(\omega) = \frac{\Omega'^{2}_{0}}{4\pi^{2} (\omega - \omega_{0})^{2}} \tag{103}$$

This function is a Lorentzian and it is symmetric about the dominant natural frequency ω_0. This power spectrum is very sharp with all the power concentrated in the ω_0 component .

One can conclude that in the free shear layer and for small disturbances of the vorticity , the component of the vorticity in the z direction is governed by a partial differential equation of the type of the heat equation . For fluctuating voticities, the z-component of the vorticity can exhibit one dominant mode in the free shear layer, if the disturbances are assumed to be weak , which provides a clear resonance signature at a frequency corresponding to the dominant mode. This is a direct and inevitable consequence of the functional form of the dependence of the fluctuations in vorticity which we have derived . Thus , the measure of the evolution of vorticity in time can provide a clear test for the existence and physical implications of dominant modes in turbulence .

IV . Conclusion

The use of laser induced fluorescence provides a new measure of density in turbulent flow whose calibration can be made including temperature effects . Such effects are multiplicative and take on a form which is proper from a quantum mechanical point of view. The use of this technique is restricted in spatial resolution only by the details of the optical set-up. It is restricted in time resolution only by the bandwidth (and the sampling rate) of the analog to digital conversion hardware.

With the density measurements achieved above, direct velocity estimations at a point are now possible for the local flow U. A three probes array is required with which, by stereoscopic reconstruction and a backward stepping approximation, all three components of U can be calculated. Furthermore, by achieving U at two points separated in x and y, one component ω_z of the vorticity can be calculated and its evolution in time at a point determined. Preliminary results based on two components direct velocity estimations, show strong signatures of Reynolds stress bursts consistent with a pronounced presence of velocity gradients in the flow.

Since strong velocity gradients as observed afford anomalous viscosity and vorticial structures, a set of a theoretical predictions for turbulent flows where this gradients are found. When $\nabla.U \neq 0$ and one has high Reynolds number reacting flow, enhanced second viscosities are possible in fully turbulent flow . Furthermore, for turbulence with dominant modes, the fluctuations in vorticity will be peculiarly sensitive with a resonance-like signature to their presence.

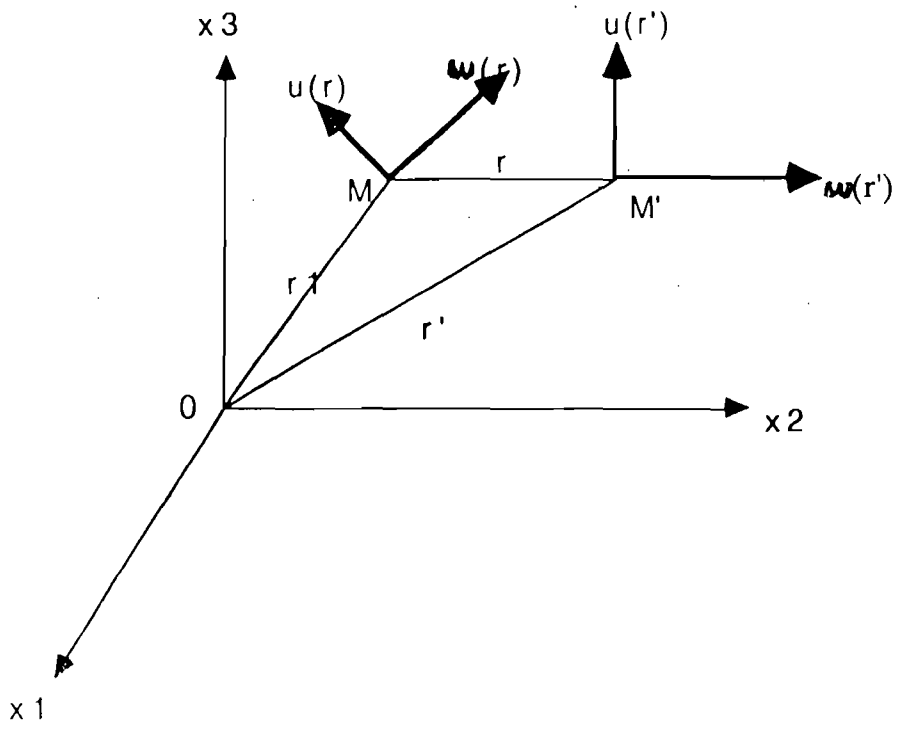

Fig.F Vorticity correlation

Contour Plot: Streaky Structures at Different Transverse Locations along the Streamwise Direction

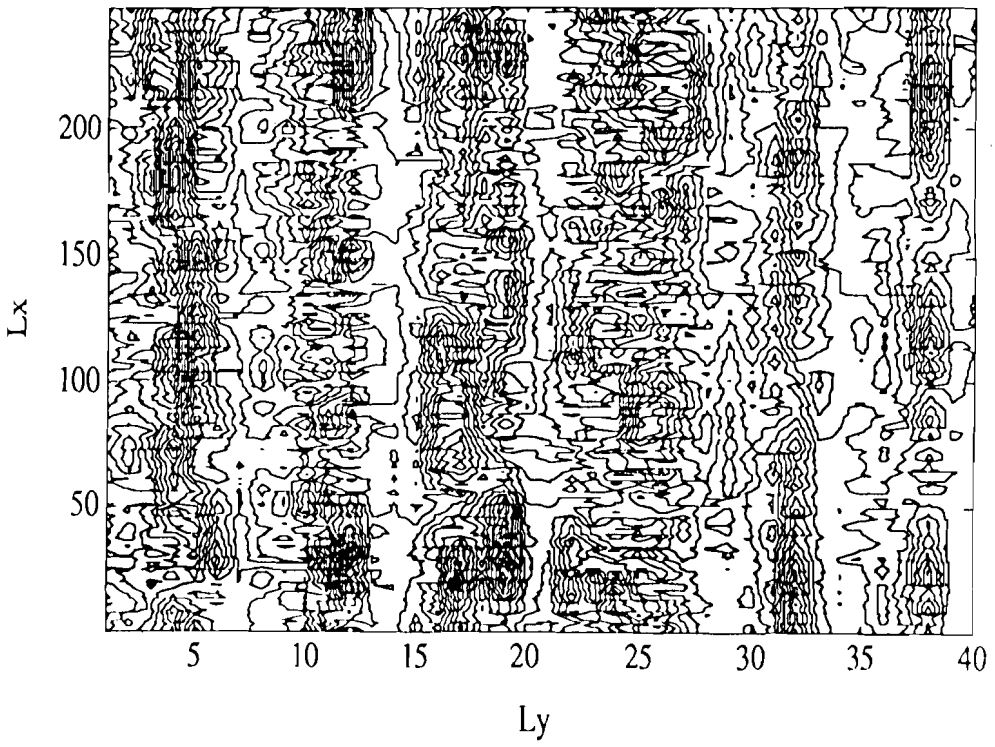

Figure 2

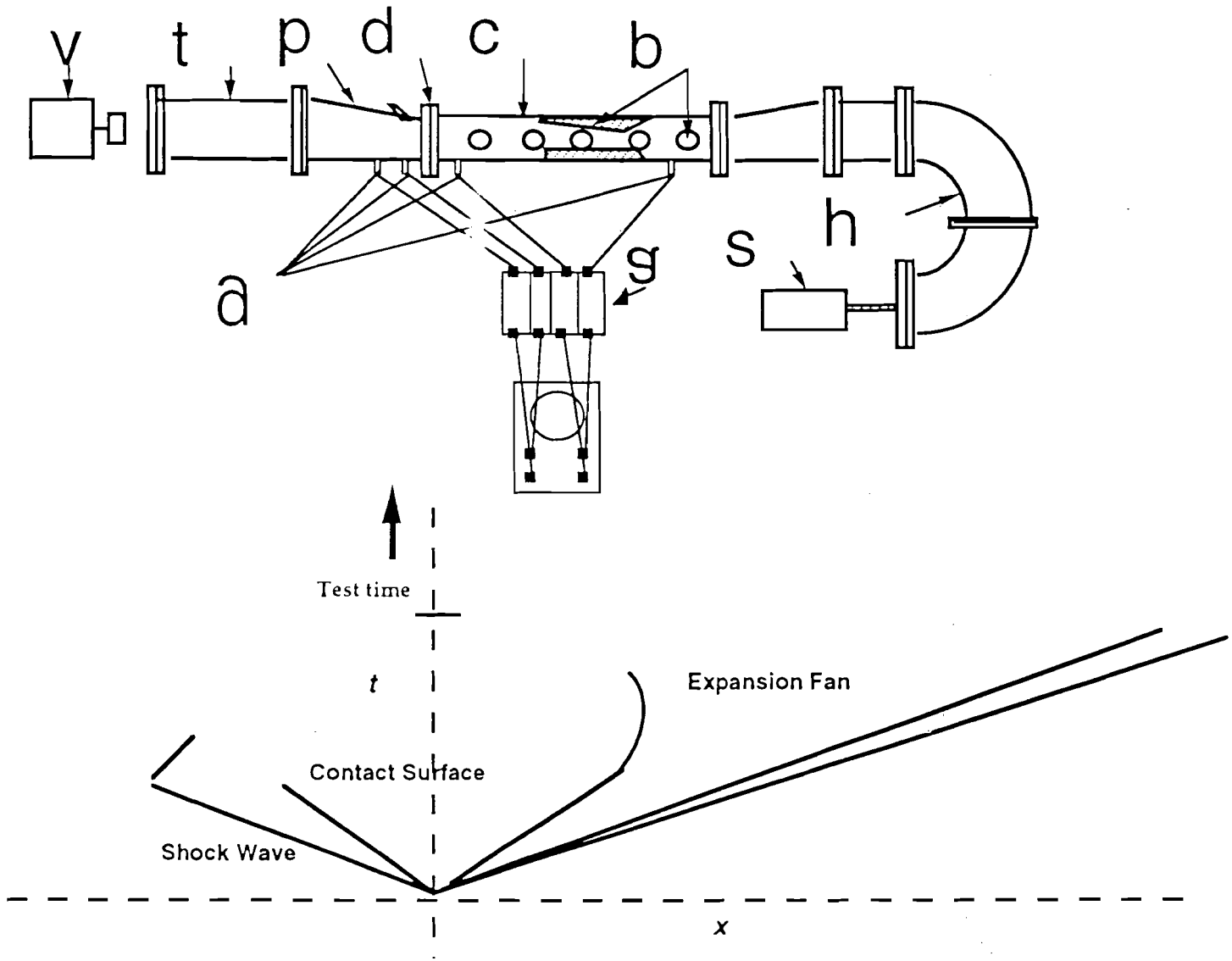
v
t
p
d
c
b
a
g
s
h
Test time
t
Expansion Fan
Contact Surface
Shock Wave
x

Figure 3

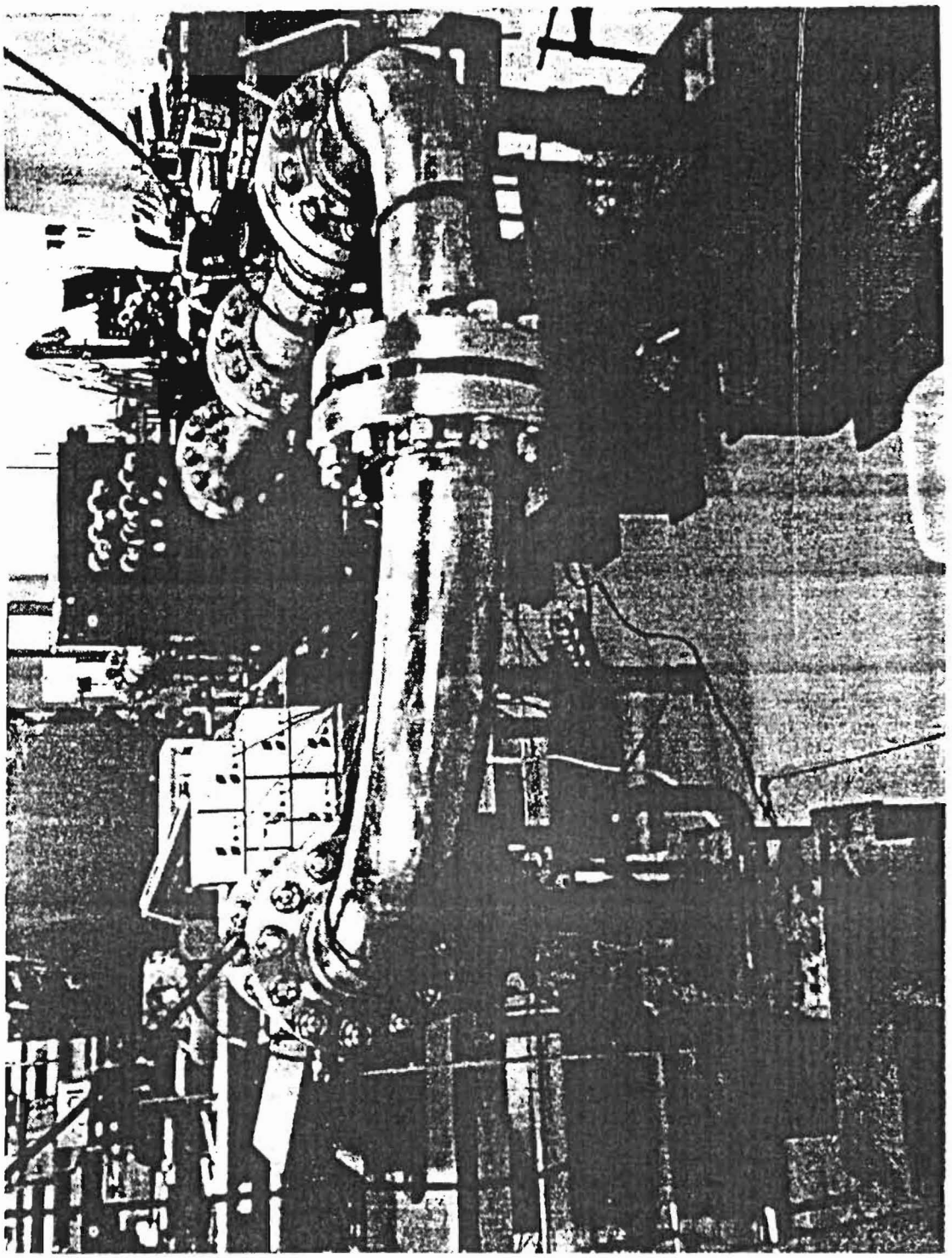

Fig. 4

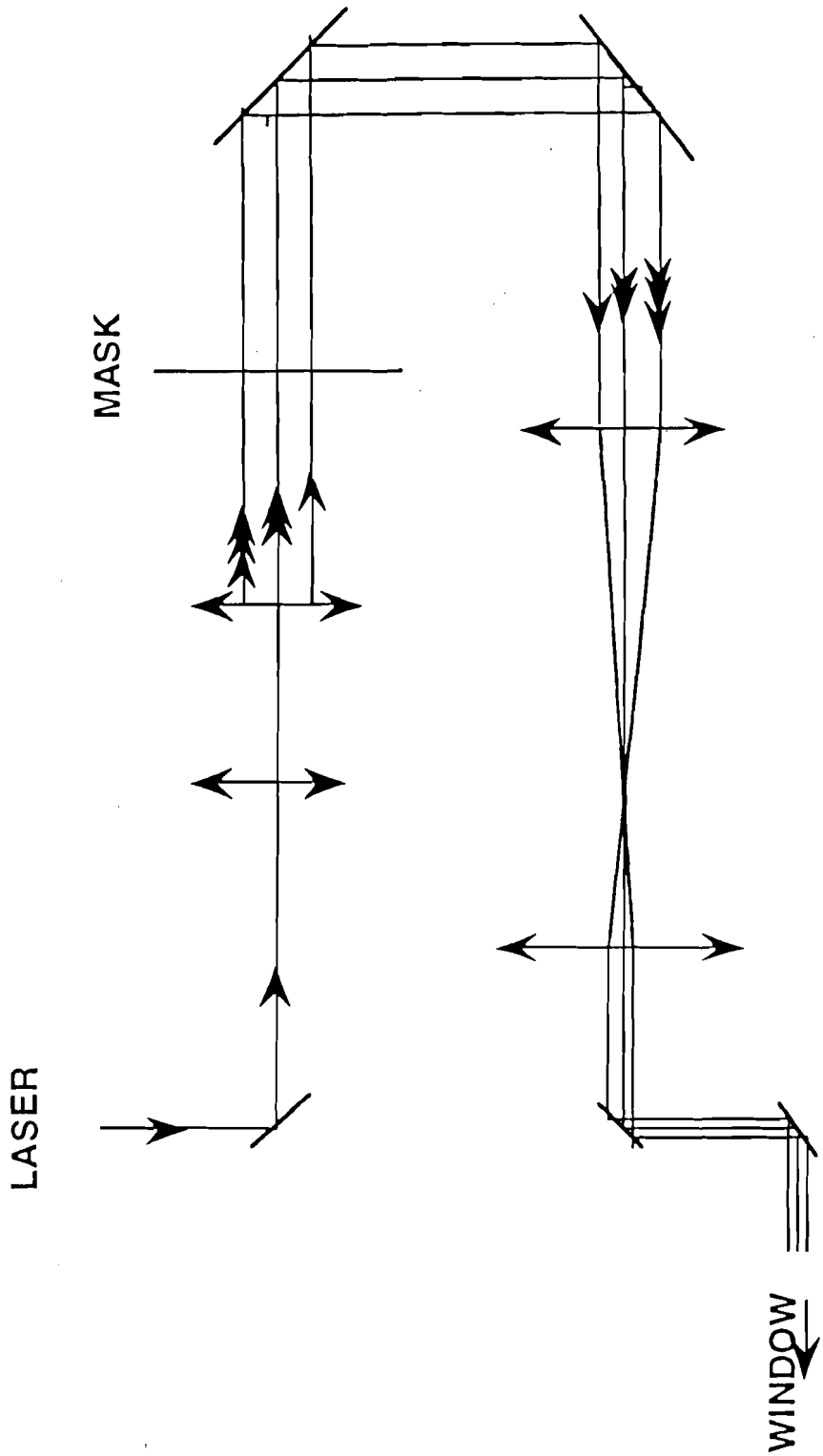

Fig. 5

Schematic of the Free Shear Layer at the Outlet Region of the Nozzle and the Center line of the Three Line Laser Beam Probes

X (mm)	5	10	15	20	25	30	35
SR	.740	.727	.714	.701	689	.676	.663
D (mm)	2.45	3.10	3.90	4.65	6.35	8.65	9.80

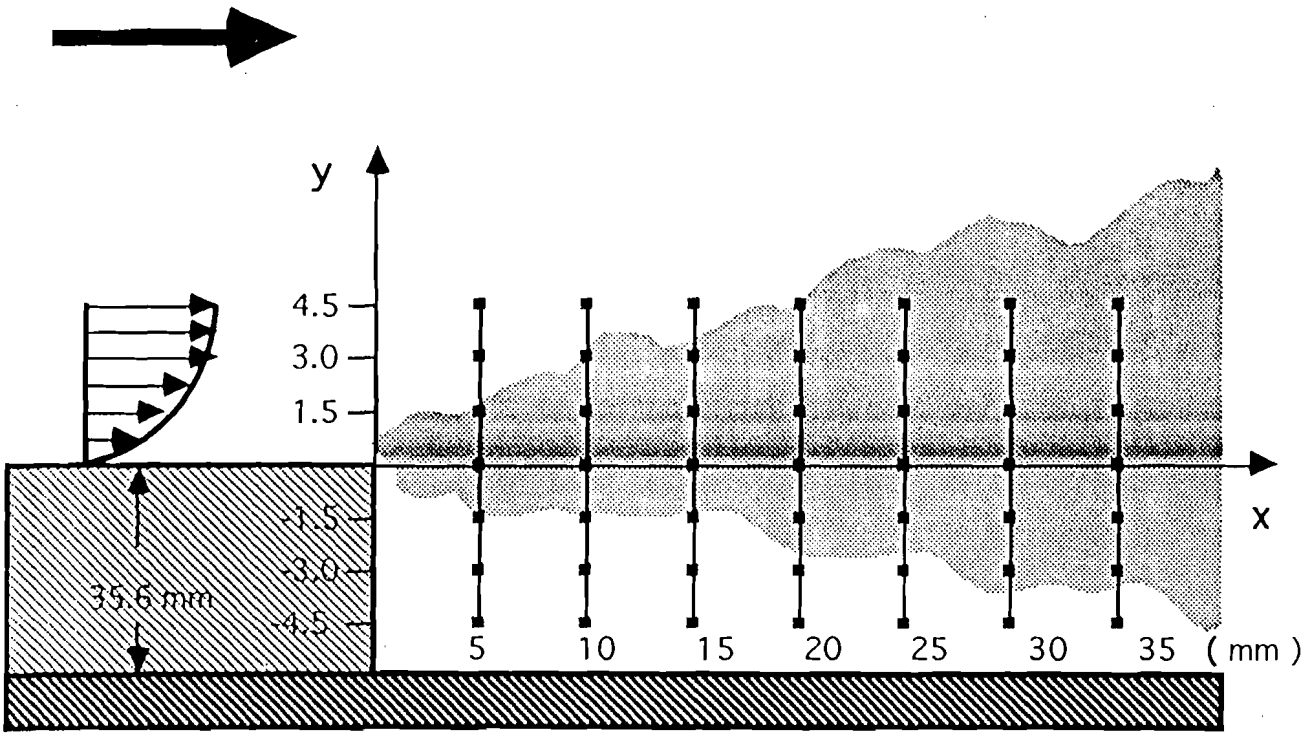

Fig. 6

OPTICAL SETUP FOR FLUORESCENCE STUDIES

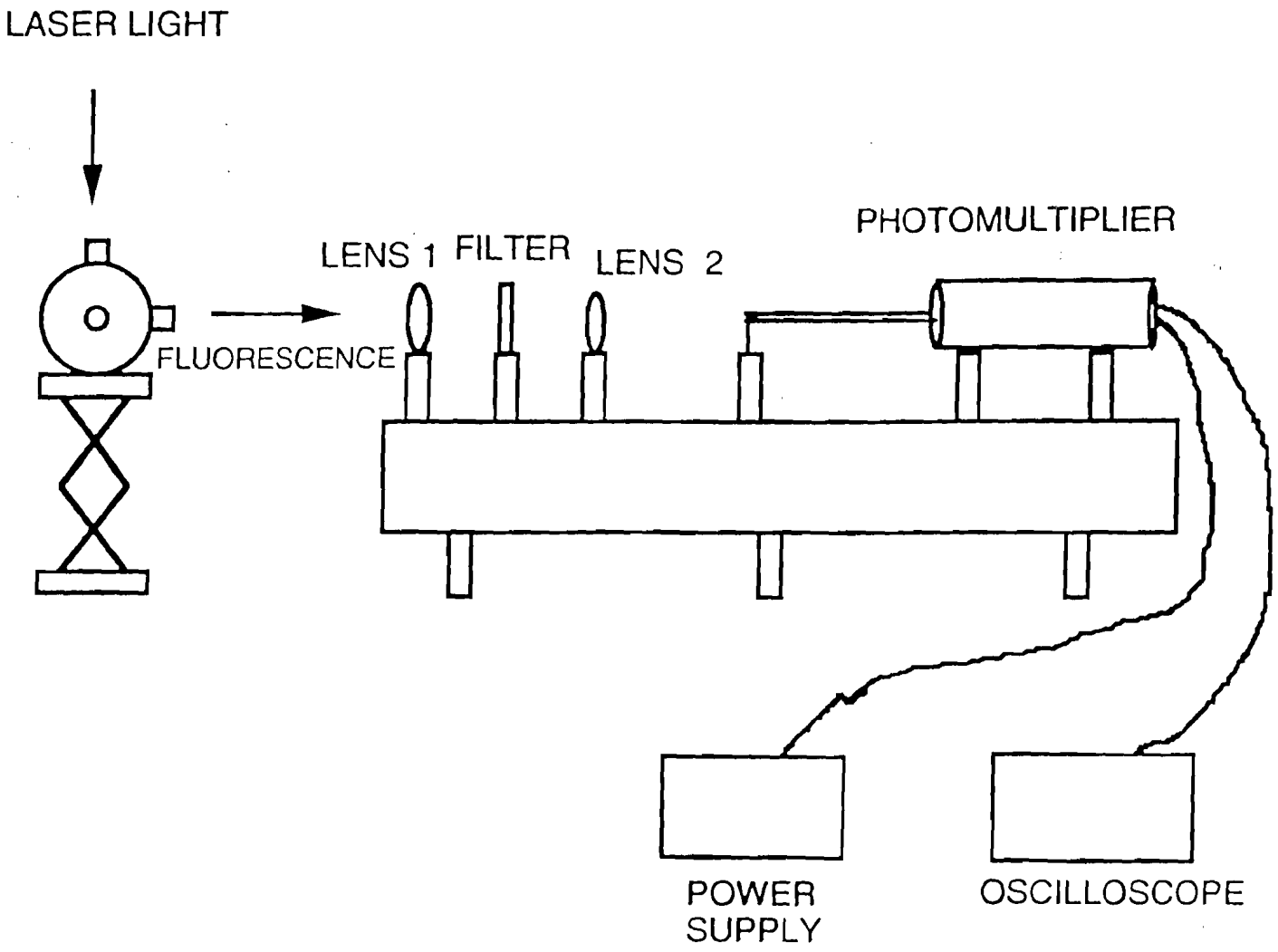

Fig. 7

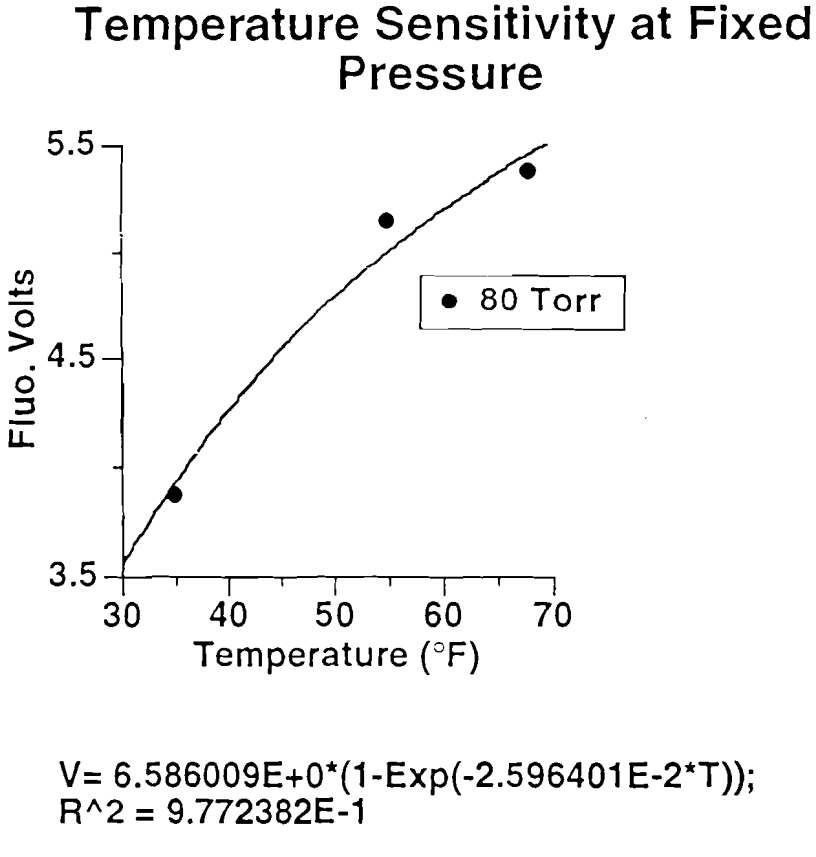
Temperature Sensitivity at Fixed Pressure
5.5
4.5
3.5
Fluo. Volts
30
40
50
60
70
Temperature (°F)
80 Torr
V= 6.586009E+0*(1-Exp(-2.596401E-2*T));
R^2 = 9.772382E-1

Fig. 8

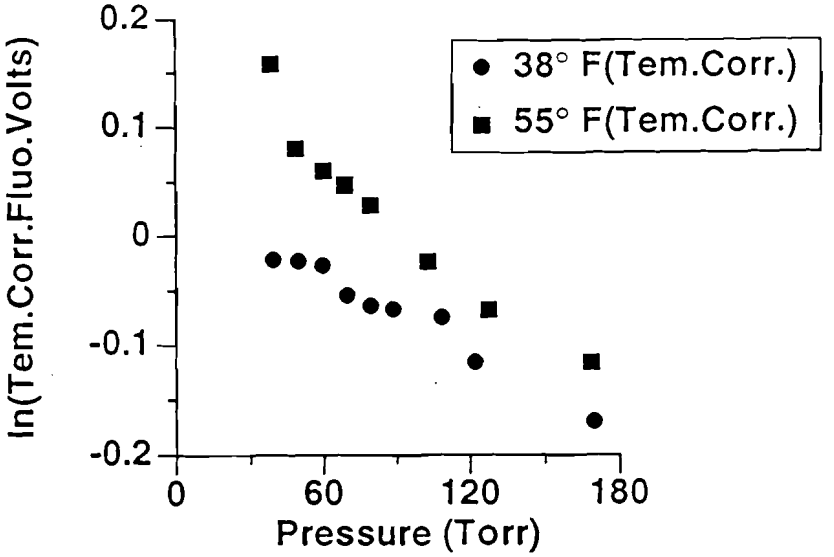
0.2
0.1
0
-0.1
-0.2
ln(Tem.Corr.Fluo.Volts)
0
60
120
180
Pressure (Torr)
38° F(Tem.Corr.)
55° F(Tem.Corr.)

Fig. 9

All Data: Temperature Sensitivity Removed

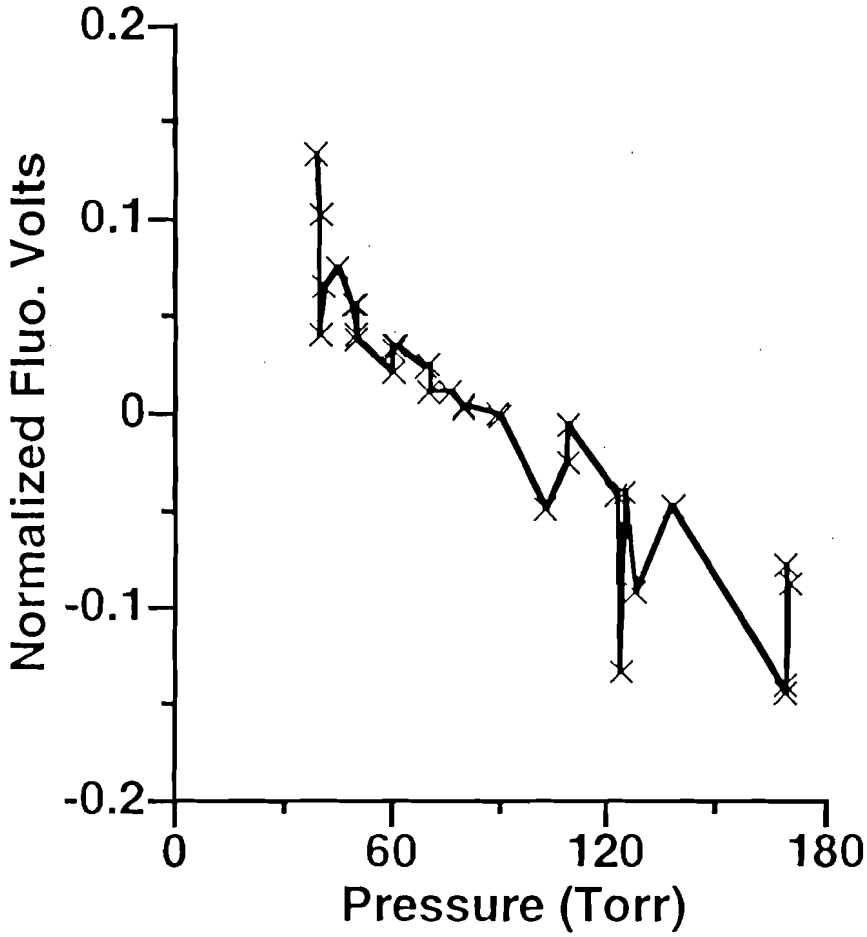

Fig. 10

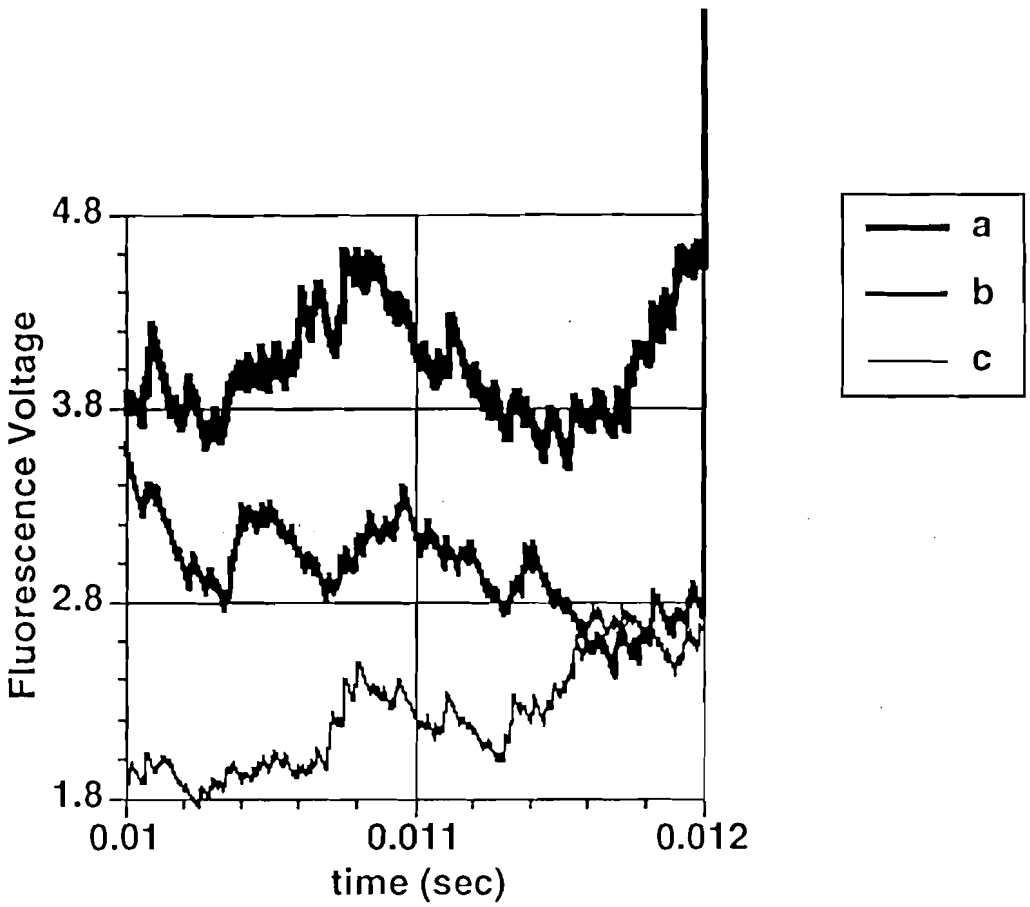

Fig. 11 :Radial Decay of Density from the Fluorescence Data

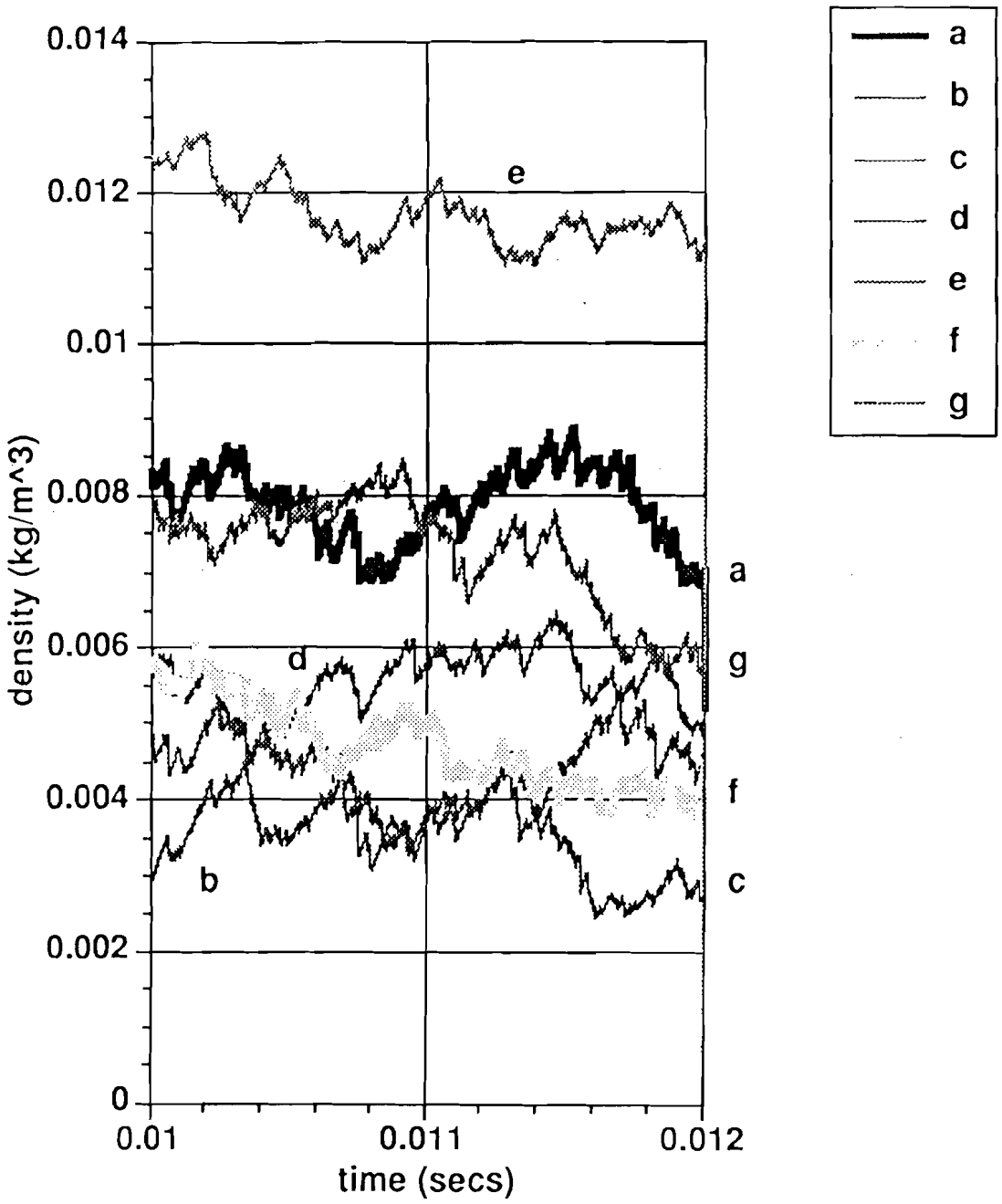
Sample of Calibrated Density Data
0.014
0.012
0.01
0.008
0.006
0.004
0.002
0
density (kg/m^3)
0.01
0.011
0.012
time (secs)
a
b
c
d
e
f
g

Fig. 12

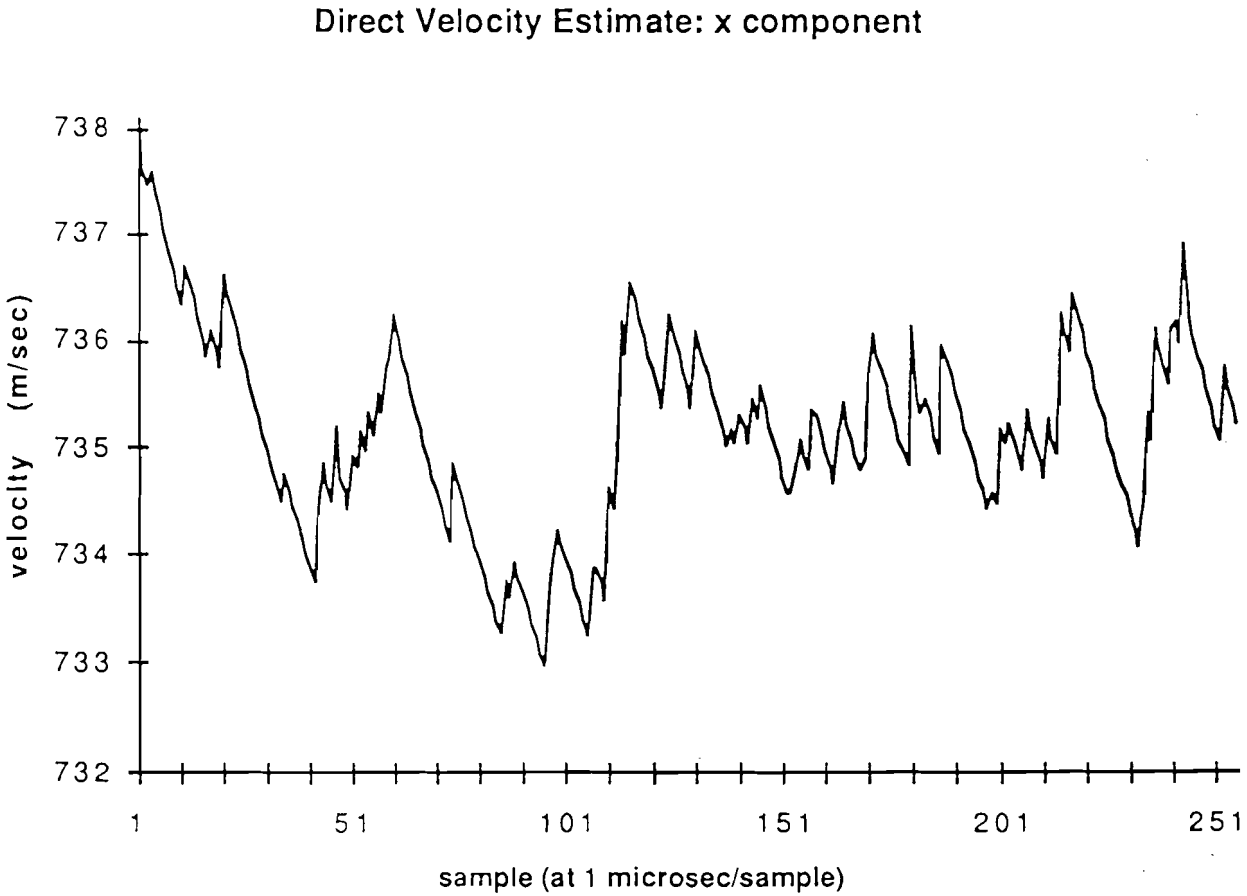
Direct Velocity Estimate: x component
738
737
736
735
734
733
732
velocity (m/sec)
1
51
101
151
201
251
sample (at 1 microsec/sample)

Fig. 13

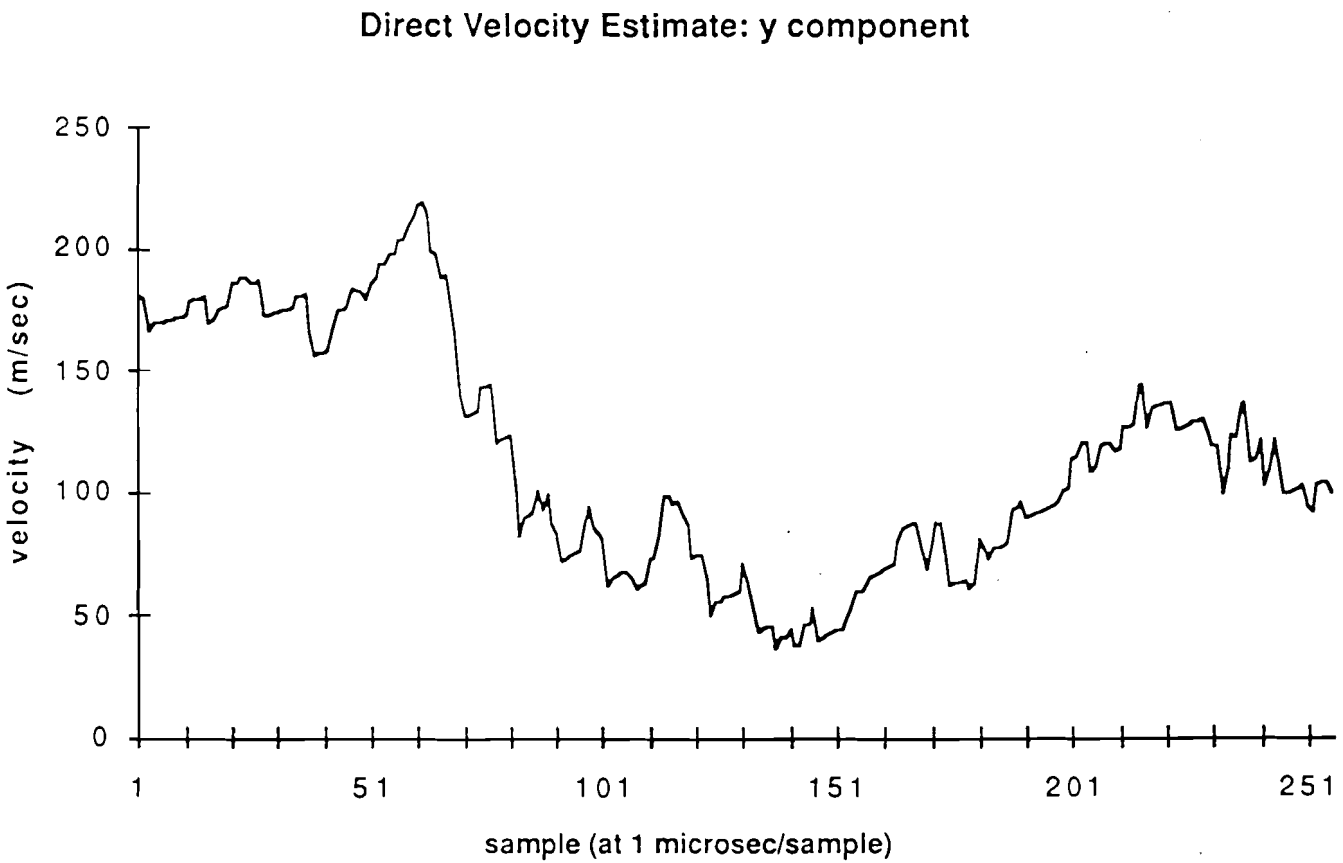
Direct Velocity Estimate: y component
250
200
150
100
50
0
velocity (m/sec)
1
51
101
151
201
251
sample (at 1 microsec/sample)

Fig. 14

First Observations: Reynolds Stress Bursts in Compressible Turbulent Flow

Fig.15

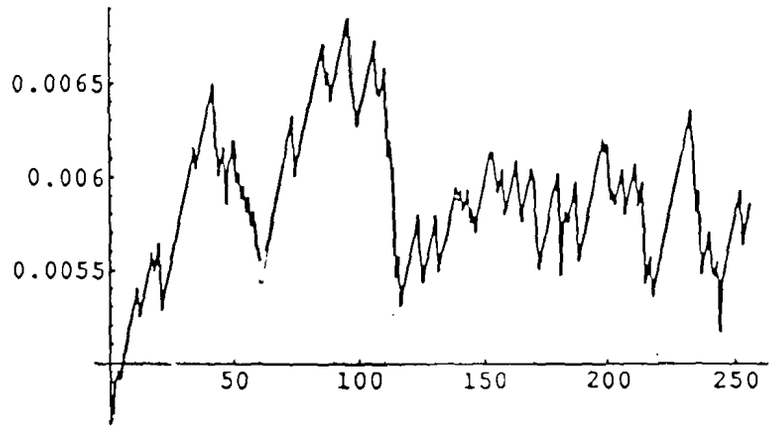

y axis:
mks units

x axis:
10^{-6}seconds

Density Profile

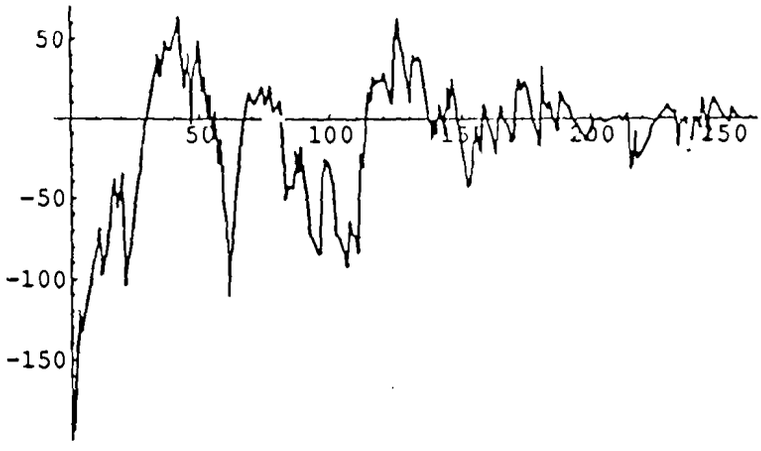

Ux*Uy; Ux and Uy velocity comp.

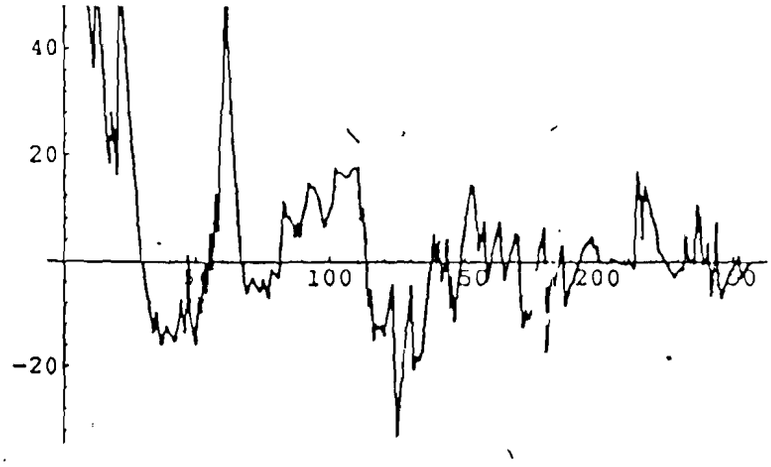

Density * Ux *Uy

References

1-Brown ,GL & Roshko , A ., 1974 On the density effects and large structures in turbulent mixing layers , J. Fluids Mech., vol.64 , p.775-816

2-Roshko, A. and Papamoschou, D., 1986 Observations of supersonic free shear layers , AIAA Paper 86-0162 .

3-M. Samimy , M.F. Reeder , and G.S. Elliott 1992 , Phys. Fluids A 4 (6) Compressibility effects on large structures in free shear flows June1992

4-Wen- Hsiung Li ; Sau-Hai Lam ; 1984 ; Principles of fluid mechanics ; Addison-Wesley Publishing Company Inc.

5- W.F. Hughes and J.A. Brighton , 1967 , Fluid dynamics ; McGraw-Hill Publishing company ; Schaum's outline series

6-A. A. Townsend , F. R. S. The structure of turbulent shear flow Cambridge University Press

7- J.O. Hinze ; 1975 , Turbulence ; MacGraw Hill book company

8-Landau L.D. and Lifshitz M., 1987 Fluid Mechanics , second edition , Pergamon Press , New York

9-A.J. Cable , and R.N. Cox , The Ludwieg pressure tube supersonic wind tunnel The aeronautical quaterly vol. XIV, Pt . 2, May 1963 pp.- 143-157

10- A. G. Gaydon and I.R. Hurle ; 1963; The shock tube in high -temperature chemical physics

11-Jianjun Zhang , 1992 , Investigation of turbulent structures in a supersonic free shear layer , PhD thesis , The City University of New-York .

12-Lee, M.J. , Kim, J. &Moin , P., 1990 Structure of turbulence at high shear rate J. Fluid Mech. vol. 216 , p;516-583

13- Richard S. Miller , The Manifestation of eddy shocklets and laminar diffusion flamelets in a shear layer , AIAA student journal 1992

14-Lele ,S.K.,1989 Direct numerical simulation of compressible free shear flows ; AIAA , paper 89-0374

15-Lee, S. , Lele, S.K., and Moin P., Eddy shocklets in decaying compressible turbulence, Phys. Fluids A, vol. 3 No 4, 1991, pp.657-664 .

16-M.M. Stanisic , The mathematical theory of turbulence (2nd edition) Springer-Verlag

17-Johnson III ,J.A., Zhang , Y . and Johnson , L.E.,1988 Evidence of Reynolds number sensitivity in supersonic turbulent shocklets, AIAA J. 26 , 502 .

18- J.K. Wright ; 1961 ; Shock tubes ; John Wiley and sons inc .

19- Paul Duchateau ,David W. Zachmann ; Partial differential equations ; Shaum's outline series in mathmatics ; MacGraw-Hill Publishing Company

20- Chorrin A.J. and Mardsen J.E. , 1979 , A mathematical introduction to fluid mechanics . Springer-Verlag

21- Elaine S . Oran and Jay P. Boris ; Computing turbulent shear flows- a conspiracy ; computer in physics ,vol. 7, No.5, sept/oct 1993

22-D. J. Tritton, Physical fluid dynamics (2nd edition) Clarendon Press . Oxford

23-G.L. Baker and J.P. Gollub , Chaotic dynamics, an introduction , Cambridge University Press

24-David K. Campbell , Nonlinear science , from paradigms to practicalities Reprinted from Los Alamos Science , Number 15 (Special issue)

25- Hwei P. Hsu ; 1984 ; Applied Fourier Analysis , Harcourt Brace Jovanovich

26-P. Bergé, Y. Pomeau , Ch; Vidal, 1984; L'ordre dans le chaos ; Hermann editeurs des sciences et des arts

APPENDIX

SECOND VISCOSITY ENHANCEMENT IN TURBULENT NONEQUILIBRIUM FLOW

by Jean Chabi Orou and Joseph A. Johnson III

CeNNAs ,Florida A&M University , Tallahassee, Florida, USA

(This paper has been published in Phys. Fluids 6 (11), January 1994)

Second Viscosity Enhancement in Turbulent Nonequilibrium Flow

Jean Chabi Orou* and Joseph A. Johnson III†

CeNNAs, Florida A&M University, Tallahassee, FL 32310

Abstract

A physical model for entropy production associated with reactive flow is presented. The general form $\chi(t) \propto (1 - e^{-\frac{t}{\tau}})$ has the correct asymptotic behaviors for t->0, t->τ and t->∞ for finite τ where τ is the relaxation time. From this, a relationship between the second viscosity and the relaxation time for A+B->P is modeled from the macroscopic entropy rate equation. Finally, using a first order approximation for reaction rate distortion from reduced molecular chaos, enhanced second viscosities can be predicted for strongly turbulent fluid systems with long relaxation times and $\nabla \bullet \vec{V} \neq 0$.

Nonmenclature

S	=entropy
s	=specific entropy
Q	=quantity of heat
T	=absolute temperature
e	=specific internal energy
A	=area
ρ	=density of the fluid
$\vec{V}$	=velocity
dv	=volume element
Φ	=dissipation function
σ	=entropy generated per unit volume per unit time

τ =relaxation time

χ =entropy generated by chemical reaction

u_x =derivative of the component of the velocity vector in x direction with respect to x

Re =Reynolds number

t =time (laboratory time)

μ =viscous stress tensor

η =dynamic viscosity

ξ =second viscosity

Introduction

It is usually assumed that the second (or bulk) viscosity and the chemical relaxation time are connected. However, the second viscosity is only relevant in processes where there is a compression or an expansion and it is usually regarded as small even when it is relevant.[1] Nonetheless, it now seems appropriate to determine in general whether or not there can be circumstances where the influence of second viscosity might be important.[2] This seems especially interesting since, in some situations, effects due to turbulence are often treated as effects due to anomalous viscosity. The present paper uses the macroscopic entropy production rate equation in a reactive flow in order to approach the possibility of a connection between the second viscosity and the relaxation time. In addition, by using the qualitative implications of recent experimental results, we will speculate on a role for turbulence in these phenomena. Generally stated, this model is proposed on intuitive arguments.

Entropy and a Relaxation Process

The total change of entropy in a system is

$$S_2 - S_1 = \int_1^2 \frac{dQ_{rev}}{T}$$

where we have assumed the system is brought from state 1 to state 2 so that

$$S_2 - S_1 = \Delta S_0 + \Delta S_i.$$

The first term in the right is the entropy carried into the system over the boundaries from outside and the second term is the entropy produced in the system during the process.

In what follows, we are going to deal with a system in which the entropy carried into the system is zero and the last term in the above equation is generated by viscosity, thermal conduction and chemical reaction. Specifically, we define σ to be the entropy per unit time and Φ to be the dissipation function. Specifically, Φ can be interpreted as the irreversible dissipation of the mechanical energy into heat caused by the viscosity per unit time per unit volume.

With these definitions, the energy balance can be expressed as follows:[3]

$$\iiint \rho\left(\frac{De}{Dt} - \frac{P}{\rho^2}\frac{D\rho}{Dt}\right)dv = \iiint (\Phi - div(\vec{q}))dv$$

where

$$\Phi = div(\vec{V}\mu) - \vec{V}div\mu$$

$$\Phi = \mu_{xx}\frac{\partial u}{\partial x} + \mu_{yy}\frac{\partial v}{\partial y} + \mu_{zz}\frac{\partial w}{\partial z} + \mu_{xy}\left(\frac{\partial u}{\partial y} - \frac{\partial v}{\partial x}\right) +$$

$$+\mu_{yz}\left(\frac{\partial v}{\partial z} - \frac{\partial w}{\partial y}\right) + \mu_{xz}\left(\frac{\partial w}{\partial x} - \frac{\partial u}{\partial z}\right)$$

in which the velocity vector $\vec{V}$ has components (u, v, w), μ is the viscous stress tensor and $\vec{q}$ is the energy flow vector. The previous equation becomes:

$$\iiint \frac{\rho}{T}\left(\frac{De}{Dt} - \frac{P}{\rho^2}\frac{D\rho}{Dt}\right)dv = -\iint \frac{\vec{n}.\vec{q}}{T}dA + \iiint\left(\frac{\Phi}{T} - \frac{\vec{q}.\nabla T}{T^2}\right)dv$$

Since

$$TdS = de - \left(\frac{p}{\rho^2}\right)d\rho$$

we now have:

$$\iiint \rho \frac{Ds}{Dt} dv = \frac{D}{Dt}\iiint \rho s dv = -\iint \frac{\vec{n}.\vec{q}}{T} dA + \iiint \sigma dv$$

where $\sigma = \left(\frac{\Phi}{T} - \frac{\vec{q}\cdot\nabla T}{T^2}\right)$.

When the entropy generated by a chemical reaction is taken into account, an additional term is required in the expression of the entropy source. The new expression for the entropy becomes

$$Tds = de - \left(\frac{P}{\rho^2}\right)d\rho + \Gamma d\chi$$

where $\Gamma = T\left(\frac{\partial s}{\partial \chi}\right)_{e,\rho}$ vanishes if the gas attains an unconstrained equilibrium at all time.

In order to derive a relationship between the additional term and the entropy source, one notices that the expression for the entropy source becomes:

$$\sigma = \frac{\Phi}{T} - \frac{\vec{q}.\nabla T}{T^2} + \frac{\rho\Gamma}{T}\frac{d\chi}{dt}$$

We will limit ourselves to the case of a chemical reaction of the type A+B—>P where A, B and P are assumed to be nonmonoatomic perfect gases[4] and χ is the entropy generated by the chemical reaction during the process. Because the reaction stops after a finite time, χ must reach a limit value which is its value at equilibrium and, at that time, the derivative of χ with respect to time becomes zero .

On the other hand, the process being irreversible, the entropy must increase from zero to the limit value in a way which agrees with the active relaxation process. Assuming that χ is only a function of time and that it satisfies the above statements, the profile of χ could be a function of the form:

$$\chi(t) \propto (1 - e^{-\frac{t}{\tau}})$$

The general behavior of $\chi=\chi(t)$ during a relaxation process would be as is shown in Fig. 1 where τ is the relaxation time. We also assume that Boltzmann's equation holds.[5]

Second Viscosity and Relaxation Time

Let's consider a chemical reaction which starts at t=0 with $\chi = 0$. Elaborating the approximation above, we assume that the value of χ becomes proportional to (1-(1/e)) at $t=\tau$ and stops when t is large enough so that $e^{-\frac{t}{\tau}}$ is almost zero. Whatever value τ has, provided it is a finite one, equilibrium will eventually be reached. If the entropy at equilibrium is independent of τ, then χ_{eq} is independent of τ and the rate of change of χ is fixed. The expression of the entropy source becomes:

$$\sigma = \frac{\Phi}{T} - \frac{\vec{q}.\nabla T}{T^2} + \frac{\rho\Gamma}{T\tau}\chi_{eq}e^{-\frac{t}{\tau}}$$

The last term is the entropy generated per unit time per unit volume by the chemical reaction .

For t fixed and a small relaxation time, the equilibrium is, of course, reached more quickly than when the relaxation time is large. For one-dimensional flow, one now finds:

$$\sigma = \frac{\frac{4}{3}\eta + \xi}{T}u_x^2 - \frac{\vec{q}.\nabla T}{T^2} + \frac{\rho\Gamma}{T\tau}\chi_{eq}e^{-\frac{t}{\tau}}$$

Next we restrict the treatment to an isolated system at a constant temperature; this restriction ignores heat released (or absorbed) by the process A + B ->P. The entropy source then becomes:

$$\sigma = \frac{\frac{4}{3}\eta + \xi}{T}u_x^2 + \frac{\rho\Gamma}{T\tau}\chi_{eq}e^{-\frac{t}{\tau}}$$

Thus the energy balance equation takes the form:

$$\iiint \rho\left(\frac{De}{Dt}-\frac{P}{\rho^2}\frac{D\rho}{Dt}\right)dv=\iiint\left(\frac{\frac{4}{3}\eta+\xi}{T}u_x^2+\frac{\rho\Gamma}{T\tau}\chi_{eq}e^{-\frac{t}{\tau}}\right)dv$$

By restricting our treatment to a perfect and nonmonoatomic gas at a constant temperature in an isolated system, the integrands in the energy balance equation cannot depend on time macroscopically. This means that the derivative of σ with respect to time must be zero and, consequently, the entropy generated by the molecular process must be balanced by a change in the viscosity. Since the second viscosity alone is free to show a change with time, it is constrained by the energy balance equation above as follows:

$$\frac{d\xi}{dt}=\frac{\rho\Gamma}{u_x^2}\frac{1}{\tau^2}\chi_{eq}e^{-\frac{t}{\tau}}$$

These results are summarized in Figs. 2 and 3. Setting $b_\xi=(\rho\Gamma\chi_{eq}/u_x^2)$, we show $\frac{1}{b_\xi}\frac{d\xi}{dt}$ vs $\frac{e^{-\frac{t}{\tau}}}{\tau^2}$ in Fig. 2. For the range in t and τ indicated, a substantial sensitivity in dξ/dt is observed; this is particularly true, for example, at low velocities u_x and high densities ρ. The relative magnitudes are indicated in Fig. 3 which is a slice through Fig. 2 at τ=30 μsec.

Notice that as the relaxation time decreases, the overall entropy change due to the chemical reaction increases. For decreasing relaxation times, there correspondingly (from the equations above) is a decreasing role for the evolution of second viscosity to play in the entropy balance.

Second Viscosity, Relaxation Time, and Turbulence

It has been observed that fully developed, as well as transitional, turbulence can be described by qualitatively predictable Orr-Sommerfeld like behaviors in the form I=I(Re, Re_{peak}) where I is the turbulent intensity and

Re_{peak} is the Reynolds number at maximum turbulent intensity.[6] It is also observed that the reaction rate decreases with increasing turbulent intensity.[7] For $\tau = \tau(Re)$ and $I = I(Re)$, we get $\tau = \tau(Re(I))$ implicitly where I is the turbulent intensity. Notice $\tau \underset{Re \to 0}{=} cnst$. Then the form

$$\tau = \tau_0 \exp\left(1 - \frac{(Re - Re_{peak})^2}{Re_{peak}^2}\right)$$

is a suitable intuitive first approximation.

This expression is now combined with the expression above for $d\xi/dt$ to achieve the behaviors shown in Figs. 4 and 5. In Fig. 4 one notices that the range of non-zero turbulent intensities increases as the value of Re_{peak} increases. A typical value for Re_{peak} would be roughly 10^6; using this value and a value of τ =30 μsec, one obtains the range of values for $d\xi/dt$ shown in Fig. 5. Here as in Fig. 2 the most dramatic changes are seen at very low values of laboratory time. Nonetheless, values for t (roughly 1 μsec < t < 40 μsec) are found during which a significant influence of relaxation time and turbulent intensity on the evolution of second viscosity is possible.

Conclusions

By using a physical model for entropy production associated with reactive flow, a relationship between the second viscosity and the relaxation time is determined from the macroscopic entropy production rate equation. This relationship enables us to predict the behavior of the second viscosity when turbulence evolves in a nonequilibrium flow. Taking advantage of previous studies which have concluded that the reaction rate decreases when turbulence increases, one can argue that the second coefficient of viscosity increases when turbulence increases.

It is difficult to normalize $\chi = \chi(t)$; therefore the results obtained here for the second viscosity as a function of the relaxation time and the Reynolds number

give only qualitative behaviors. Nonetheless, a relationship has been established between the second viscosity and the relaxation time for a nonequilibrium process. We have shown how this relationship can lead to a dependence of the second viscosity on turbulence. For a flow where $\nabla \bullet \vec{V} \neq 0$, anomalous viscous effects can therefore be expected, under some circumstances, for turbulent nonequilibrium systems.

Acknowledgements

This work was supported in part by NASA Grant NAGW-2930.

References

* Research Assistant. Also Graduate Student, IMSP/Université Nationale du Benin, Cotonou, Benin.

† Distinguished Professor of Science and Engineering, Professor of Physics and Mechanical Engineering. Assoicate Fellow AIAA.

[1]Landau, L and Lifshitz, E., Fluid Mechanics, Pergamon Press, New York, 1987, pp 44-94 and pp 308-312.

[2]Emanuel, G., "Effect of Bulk Viscosity on a Hypersonic Boundary Layer," Physics of Fluids A, Vol. 4 , No. 3, 1992, pp. 491-495

[3]Becker, E.. Gas Dynamics, Academic Press, New York, 1968, pp 1-70.

[4]Clarke, J. F. and McChesney, M. The Dynamics of Real Gases, Butterworths, London, 1964, pp. 100-274.

[5]Vincenti, W. and Kruger, C., Introduction to Gas Dynamics, John Wiley & Sons, Inc., New York, 1965, pp. 328-333.

[6]Johnson, J, Lin I and Ramaiah, R., 'Reduced Molecular Chaos and Flow Instability, in "Stability in the Mechanics of Continua (F. H. Schroeder, ed.), Springer-Verlag, Berlin, 1982 pp 318-329.

[7]Johnson, J. A. III, Johnson, L. E., and Lu, X.-N., "Turbulence in a Reacting Contact Surface," Physics of Fluids A, Vol. 2, No. 11, 1990, pp. 2002-2010.

Figure Captions

Figure 1. A Model for the Entropy Generation Term Resulting from a Chemical Process.

Figure 2. The Sensitivity of the Rate of Change in Second Viscosity ($d\xi/dt$) to Changes in Laboratory Time (t) and Chemical Relaxation Time (τ).

Figure 3. A Slice through the Contour Plot in Fig. 3 at $\tau = 30$ μsec.

Figure 4. The Sensitivity of Turbulent Intensity to Changes in Reynolds Number. Turbulent Intensity is indicated by Int and Re_{peak} is the value of the Reynolds number at peak turbulent intensity as discussed in Ref. 6.

Figure 5. The Sensitivity of the Rate of Change in Second Viscosity ($d\xi/dt$) to Changes in Laboratory Time (t_{lab}) and Reynolds Number. A value of $Re_{peak} = 1.0 \times 10^6$ is used for this contour plot.

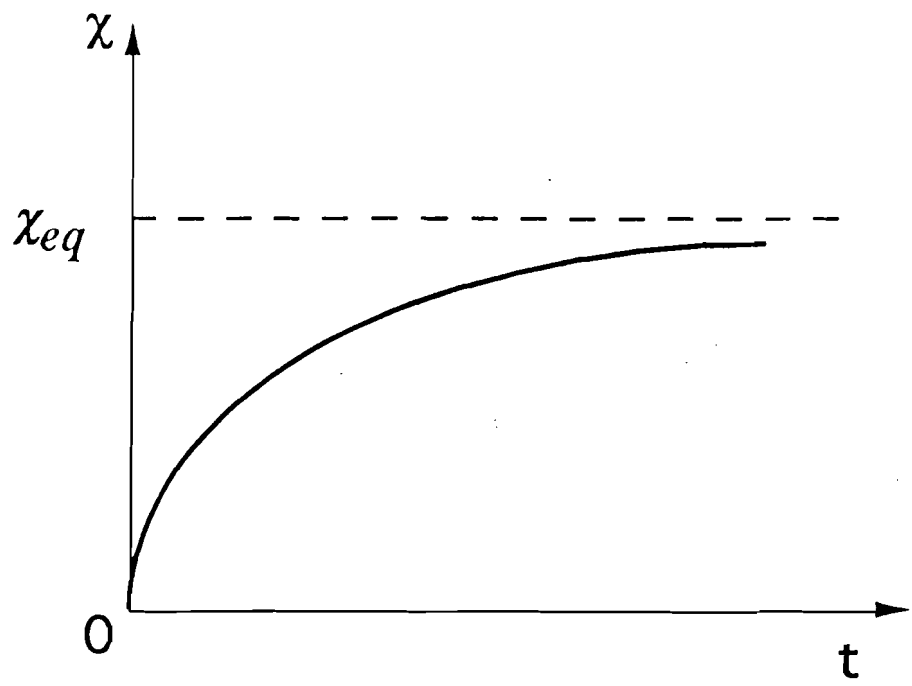

Fig. 1

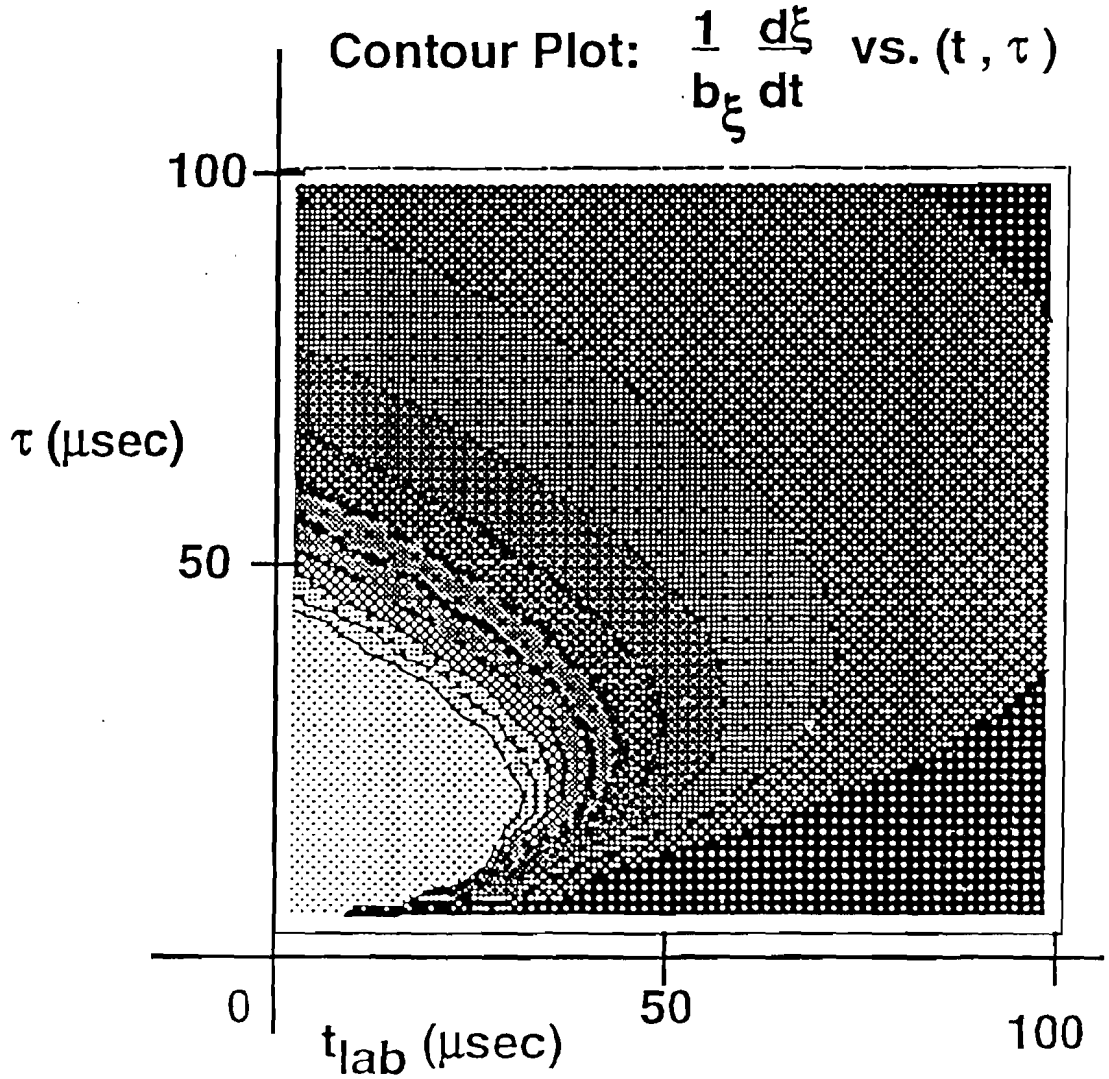
Contour Plot: $\frac{1}{b_\xi}\frac{d\xi}{dt}$ vs. (t , τ)
100
τ (μsec)
50
0
50
100
t_{lab} (μsec)

Fig. 2

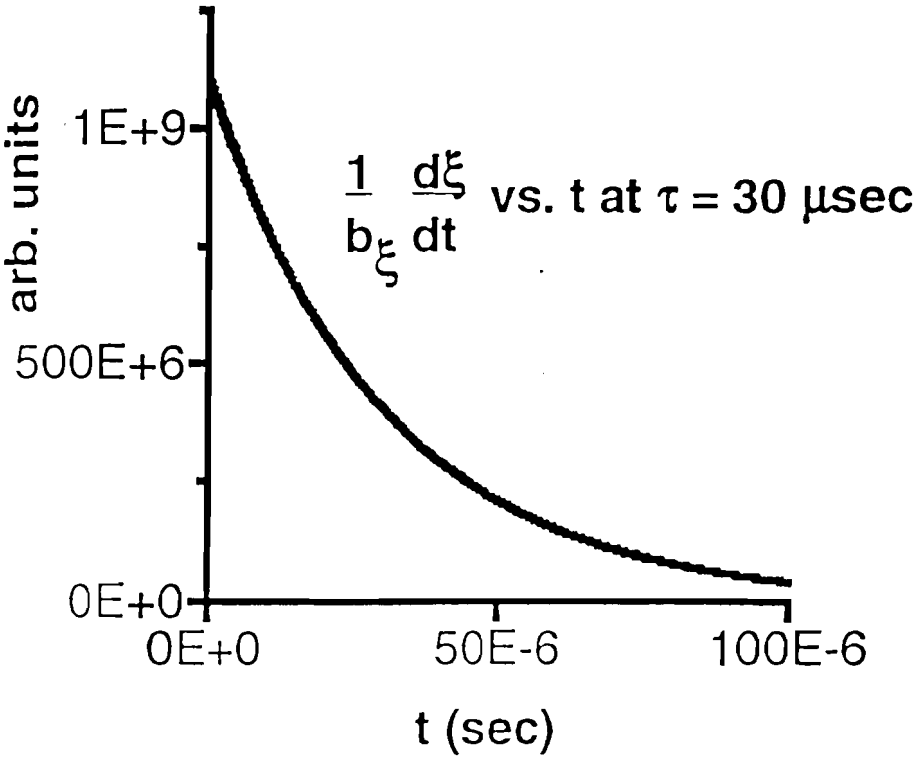
arb. units
1E+9
500E+6
0E+0
0E+0
50E-6
100E-6
t (sec)
1/b_ξ dξ/dt vs. t at τ = 30 μsec

Fig. 3

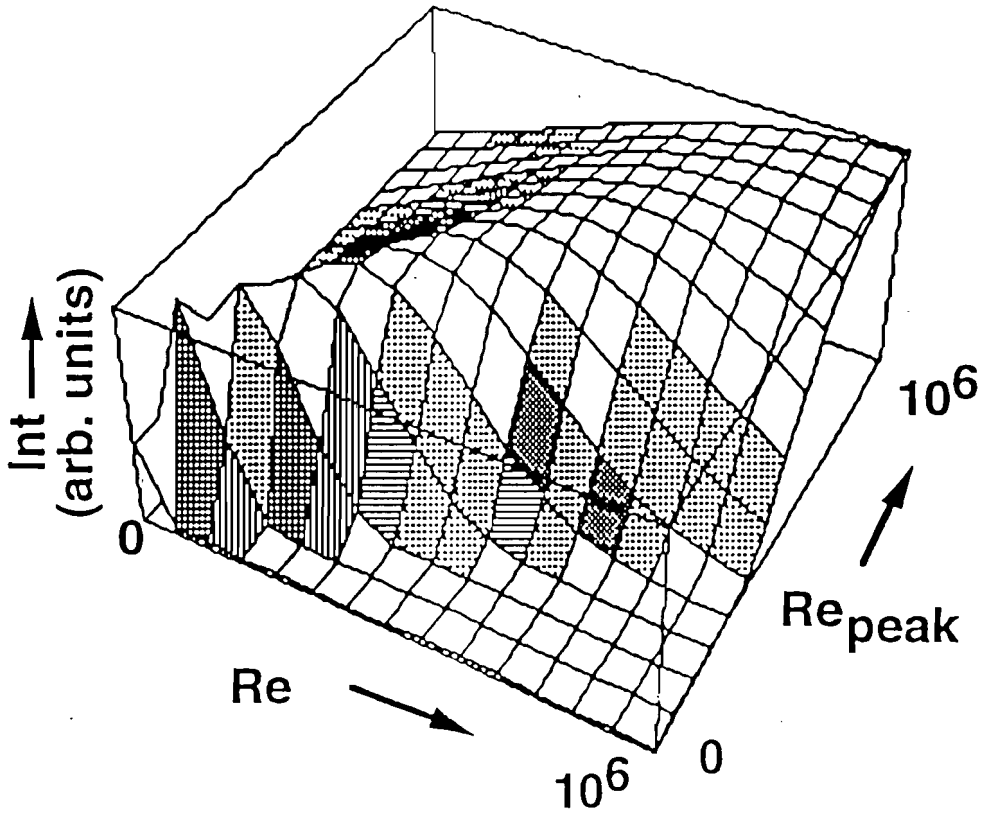

Fig. 4

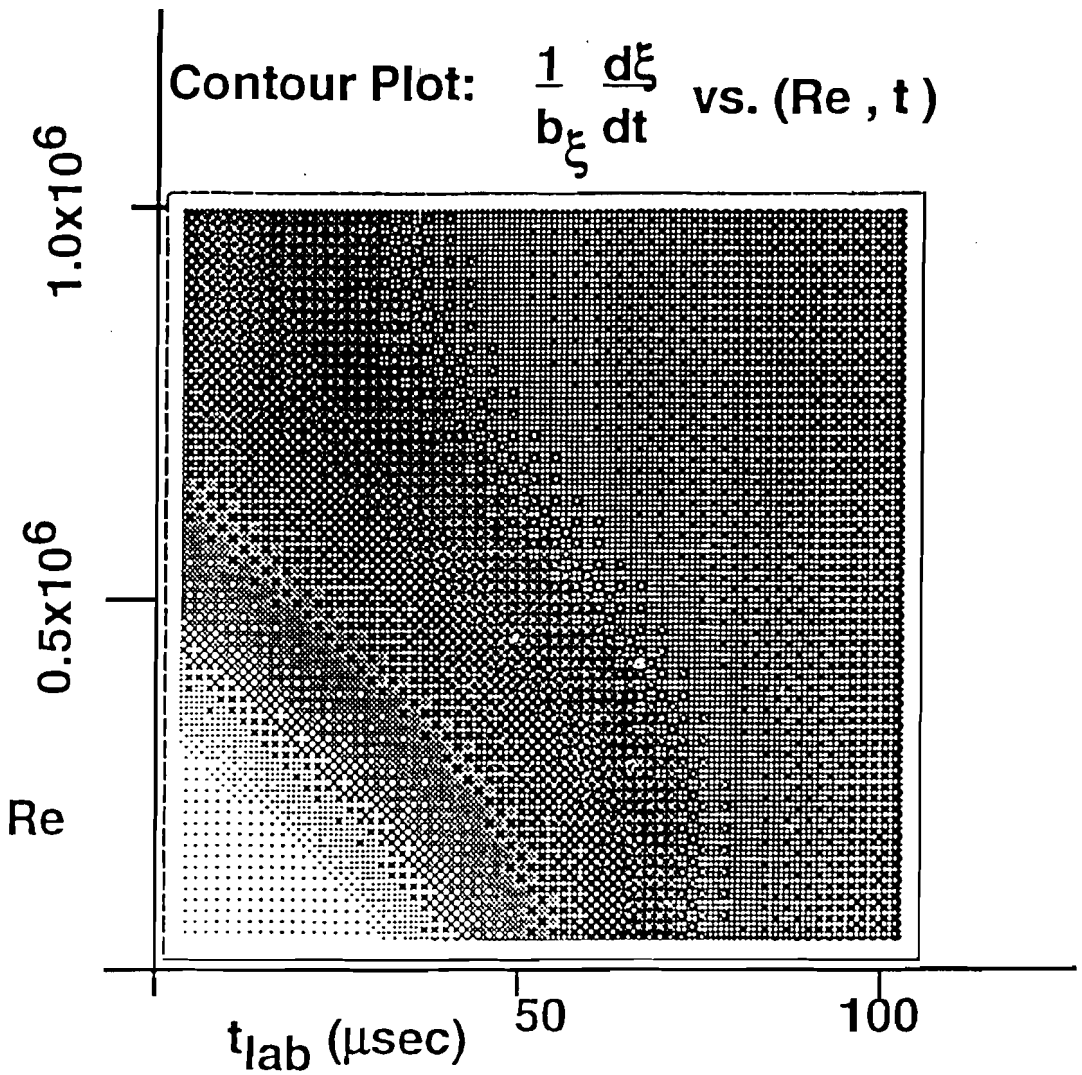
Contour Plot: $\frac{1}{b_\xi}\frac{d\xi}{dt}$ vs. (Re , t)
1.0x10^6
0.5x10^6
Re
50
100
t_lab (μsec)

Fig. 5

Part B

A THEORY OF HOMOGENEOUS CONDENSATION

Abstract

In this study of the theory of homogeneous condensation , we have proposed another approach beyond the classical theory of homogeneous nucleation. A stochastic model has been proposed for the droplet growth. We start from the Landau-Ginsburg theory , we have obtained a Langevin type equation. The Langevin type equation for the radius of the nucleus is transformed to a Fokker-Planck equation for the distribution function .We calculate the number of simple water molecules that can be fixed by the isolated liquid droplet from which the probability P(r) of finding water within a given volume around the critical droplet is computed. P(r) is not strictly zero inside the critical radius a ;it's the soft core model. In the hard core model the rate of growth of the droplet has been found analytically whereas in the soft core model the rate of growth can be found only numerically .

A THEORY Of HOMOGENEOUS CONDENSATION

I-Introduction

A great deal of experiments has been done on condensation of gases in nonequilibrium flows especially in cloud chambers and with supersonic nozzles [1] ,[2]. At the Center for Nonlinear and Nonequilibrium Aeroscience (CeNNAs), a special interest has been focusing recently on the turbulence at the contact surface in the shock tube [3], and evidences of condensation of water at the contact surface have been found using the light scattering technique [4] .

On the theoretical side, there is a classical theory of homogeneous nucleation of water vapor condensation but limits have been found for this theory [5]. First of all, we present the background which allows us to describe the classical theory. Then we will present a soft core stochastic model for the droplet growth, followed by a hard core model. Finally we will discuss how this theory can improve our knowledge about homogeneous condensation in different phenomena such as dew formation, clouds, rains and thin film growth.

II- BACKGROUND

In absence of seeds (soot, dust) let us consider a cloud of water vapor containing supersaturated vapor. To understand the meaning of a supersaturated vapor, let us look at the P,T thermodynamic diagram (Fig. B1); we find far from the critical region the following behavior

The Clausius - Clapeyron equation gives the equation of the saturated line such that

$$\ln P_{\infty}(T) = - \frac{A}{T} + B \tag{1}$$

The Clausius -Clapeyron equation reads

$$\frac{dP_{\infty}(T)}{dT} = \frac{L(T)}{\Delta V\, T} \tag{2}$$

A and B are constants

$L(T)$ is the heat of vaporisation

ΔV is the difference of volume between the liquid and the gas phases

$P(T)$ the isentropic line (constant entropy and adiabatic process) crosses the saturation line somewhere at $S = 1$ where S is the saturation ratio.

$$S = \frac{P(T)}{P_{\infty}} \tag{3}$$

At $S = 1$ the vapor is saturated with 100% humidity and when S is greater than 1 the vapor is supersaturated with no appearance of condensation. In general, an adiabatic process follows Poisson law

$$\frac{dP}{dT} = \frac{\gamma}{\gamma - 1} \frac{P}{T} \tag{4}$$

where

$$\gamma = \frac{C_p}{C_v} \tag{5}$$

C_p is the specific heat at constant pressure

C_v is the specific heat at constant volume

Then

$$\frac{P}{P_0} = \left(\frac{T}{T_0}\right)^{\frac{\gamma}{\gamma-1}} \qquad (6)$$

III - Classical theory of homogeous nucleation (Becker-Doring theory

Now how come water vapor becomes a liquid water droplet? We will present now the classical theory of homogeneous nucleation[6].

We assume two main steps . Firstly there is the formation of a water droplet of critical size , secondly the growth process of the water droplet . And the present study will only deal with the second step, that is the growth of the water droplet.

We will briefly describe the first step. In a cloud volume of supersaturated water vapor, the molecules of water are attracted together and may form clusters of a number of individual molecules. These clusters are not stable until they reach a critical size whose critical radius is r^* .

If a cluster does not reach the critical size it eventually disappears and the water molecules are scattered in the supersaturated bath. The critical radius r^* is given by

$$r^* = \frac{2\sigma}{\rho_c\left(\frac{R}{\mu}\right) T \ln S} \qquad (7)$$

σ is the surface tension

ρ_c is the critical density of water

R is the ideal gas constant

μ is the molecular weight of water

When the critical size is reached, the droplet can grow.
There are two main approaches for the theory of the droplet growth: a deterministic one and a stochastic one , but both lead to the same type of results [6].

The growth rate $\frac{dr}{dt}$ is constant (Thompson law). It can be expressed as follows

$$\frac{dr}{dt} \approx \frac{P(T) - P_\infty(T)}{\left[2\pi\left(\frac{R}{\mu}\right) T\right]^{\frac{1}{2}}} \tag{8}$$

or as

$$r(t) = \left(\frac{dr}{dt}\right) t + r^* \tag{9}$$

The nucleation rate I follows the Eyring law

$$I = \Omega \exp - \frac{W^*}{k_B T} \tag{10}$$

where

k_B is the Boltzman constant

W^* is the energy barrier

Ω is the statistical prefactor called the frequency factor

The mechanisms of growth are evaporation and condensation of simple water molecules on the surface of the droplet, diffusion of droplets and coalescence of several droplets colliding together. There is W^* an activation energy which is a usual ingredient in these theories [7]. The Arrhenius exponential factor gives the dominant contribution. I the nucleation rate represents the number of critical size droplets formed per unit time and per unit volume. In 1939 Volmer [5] showed that

$$I = \left(\frac{2}{\pi}\right)^{1/2} \frac{N_A^{3/2}}{R} \left(\frac{P}{T}\right)^2 \frac{(\sigma\mu)^{1/2}}{\rho_c} \exp - \frac{4\pi(r^*)^2\sigma}{3k_BT} \tag{11}$$

where N_A is the Avogadro number.

We can immediatly see that the activation energy is given by

$$W^* = \frac{4}{3}\pi r^{*2}\sigma \tag{12}$$

In nonequilibrium flows we have in general $P(t)$ and $\rho(t)$. The pressure and the density of the gas involved are time independent therefore the nucleation rate is time dependent: $I(t)$. Finally the condensate mass fraction $l(t)$ obeys to the following rate equation

$$\frac{dl}{dt} = f(P,T,l)$$

$$\frac{dl}{dt} = 4\pi\rho_c \left[\frac{I(t)}{\rho(t)} \frac{r^{*3}(\tau_0)}{3} + \frac{dr}{dt} \int_0^t \frac{I(\tau)}{\rho(\tau)} \left[r^*(\tau_0) + \int_{\tau_0}^{\tau} \frac{dr}{d\theta} d\theta \right]^2 d\tau \right] \tag{13}$$

We also have the case where $P(x,t)$, $\rho(x,t)$, $I(x,t)$, $l(x,t)$ are position and time dependent functions.

We would like now to present some new approaches of the theory of droplet growth. The results are that $\frac{dr}{dt}$ is no more a constant but is time dependent.

IV- Soft core stochastic model for the droplet growth (Chandrasekhar-Hertz [8])

This model was used for the stellar distribution theory, a nearest neighbour random distribution of stars. We assume a liquid droplet of critical radius $\mathbf{r^*= a}$ bathing in water vapor. Then consider the droplet of radius a forming a core which cannot be penetrated by simple water molecules coming close to the surface of the droplet. $w(r)$ the distribution of simple molecules around the isolated spherical droplet is given by

$$w(r) = \left[1 - \int_0^r w(r')dr' \right] 4\pi r^2 \tag{14}$$

yielding

$$w(r) = \exp\left(-\frac{4\pi r^3}{3}\right) 4\pi r^2 \tag{15}$$

If dN is the number of simple water molecules in the shell between r and r+dr, and $dv = 4\pi r^2 dr$ is the elementary volume of the shell

$$dN = k \exp\left(-\frac{4\pi r^3}{3}\right)4\pi r^2 dr \tag{16}$$

Which leads to

$$N = 4\pi k \int_a^{\infty} \exp\left(-\frac{4\pi r^3}{3}\right) r^2 dr \tag{17}$$

Thus

$$N = k \exp\left(-\frac{4\pi a^3}{3}\right) \tag{18}$$

N is the total number of water molecules that can be fixed by the isolated liquid droplet.

k being a proportionality constant between dN and dv

$$\frac{dN}{N} = df(r) = \Pi(r)dr = \frac{k \exp\left(-\frac{4\pi r^3}{3}\right)4\pi r^2 dr}{N} \tag{19}$$

is the probability of finding liquid water within a given volume element dv around the critical droplet.

Then the distribution function is

$$\Pi(r) = 4\pi r^2 \exp(-4\pi/3(r^3 - a^3)) \tag{20}$$

The distribution function has the required form and one can see that $\Pi(r)$ tends to zero when r tends to zero , but inside the critical radius a, $\Pi(r)$ is not strictly zero, that is the soft core model (Fig. B-2).

We will study now some useful properties of this distribution function.

$$\frac{d}{dr}\Pi(r) = \left[1-2\pi r^3\right]8\pi r \exp - \frac{4\pi}{3}(r^3 - a^3)$$

(21)

$$= 0$$

The solutions are

$$r = \frac{1}{2\pi^{1/3}} \text{ for } \Pi_{max}$$

$$r = 0 \text{ for } \Pi_{min} \tag{22}$$

$$r \to \infty \text{ for } \Pi_{min}$$

$$\bar{r} = \int_a^{\infty} r\,\Pi(r)dr = \left(\frac{3}{4\pi}\right)^{1/3}\exp\frac{4\pi a^3}{3}\int_{4\pi a^3/3}^{\infty} U^{1/3}\exp - U dU$$

(23)

$$\bar{r} = \left(\frac{3}{4\pi}\right)^{1/3}\exp 4\pi a^3\,\Gamma\left(\frac{4}{3}\right)\left[1 - I\left(\frac{4}{3}, \frac{4\pi a^3}{3}\right)\right] \tag{24}$$

where

$$\Gamma(m) = \int_0^{\infty} e^{-t}\,t^{(m-1)}dt \tag{25}$$

m is real

$$I(m,z) = \frac{1}{\Gamma(m)} \int_0^z e^{-\tau} \tau^{(m-1)} d\tau \qquad (26)$$

$\Gamma(z)$ is the gamma function and $I(m,z)$, the incomplete gamma function.

Let us put $a \approx 0$ to give an idea of the value of $\bar{r}$

$$\bar{r} = \int_0^\infty r\, \Pi(r) dr = \frac{\Gamma(4/3)}{(\frac{4\pi}{3})^{1/3}} \exp \frac{4\pi a^3}{3} \qquad (27)$$

But the exact value of $\bar{r}$ is

$$\bar{r} = \frac{\Gamma(4/3)}{(\frac{4\pi}{3})^{1/3}} \exp \frac{4\pi a^3}{3}\, g(a) \qquad (28)$$

where

$$g(a) = \left[1 - I(\frac{4}{3}, \frac{4\pi a^3}{3}) \right] \qquad (29)$$

Let us now extract $\frac{dr}{dt}$ for $r \sim \bar{r}$ to characterize the droplet growth. From expression (19) we can write

$$\frac{dr}{dt} = \frac{1}{\Pi(\bar{r})} \frac{df(\bar{r})}{dt} \qquad (30)$$

Now it remains to calculate $\frac{df(\bar{r})}{dt}$ independently

$$\frac{df(\bar{r})}{dt} \approx \frac{dv}{v}\frac{1}{dt} = \frac{d}{dt}\ln(v) = \frac{d}{dt}\ln\left(\frac{4\pi\bar{r}^3}{3}\right) \tag{31}$$

$$\frac{df(\bar{r})}{dt} = 3\frac{d}{dt}\ln(\bar{r}) = 4\pi\frac{dr^{*3}}{dt} + 3\frac{d}{dt}\ln g(r^*) \tag{32}$$

$a = r^*$ is the critical radius

Let us write

$$A = \frac{2\sigma}{\rho_c \frac{R}{\mu} T} \tag{33}$$

If

$$r^* = \frac{A}{\ln\frac{P}{P_\infty}} \tag{34}$$

Then

$$\frac{dr^*}{dt} = -\frac{r^{*2}}{A}\frac{d}{dt}\ln P \tag{35}$$

The calculation gives

$$r(t,t_0) = r^{*}(t_0) + \int_{t_0}^{t} \frac{dr}{d\theta}\, d\theta \tag{36}$$

$$r(t,t_0) = r^{*}(t_0) + \frac{3}{5\bar{r}^{-2}} \exp \frac{4\pi \bar{r}^{-3}}{3} \left[\frac{r^{*3}(t)}{\left[\ln \frac{P(t)}{P_\infty}\right]^2} - \frac{r^{*3}(t_0)}{\left[\ln \frac{P(t_0)}{P_\infty}\right]^2} \right] \tag{37}$$

with

$$\bar{r} \approx \frac{\Gamma(\frac{4}{3})}{(\frac{4\pi}{3})^{1/3}} \exp \frac{4\pi r^{*3}}{3} g(r^{*}) \tag{38}$$

We might need to introduce as in the case of stellar distribution n_0 the number of vapor water in the medium , then

$$w(r) = \left[1 - \int_0^r w(r')dr' \right] 4\pi r^2 n_0 \tag{39}$$

Thus

$$w(r) = (\exp - \frac{4\pi r^3}{3} n_0) 4\pi r^2 n_0 \tag{40}$$

Then the results are changed only slightly and are then more general.

V- HARD CORE MODEL

Now we assume that $\Pi(r) = 0$ strictly inside the core, it is the hard core model instead of the soft core model described earlier. Again we consider dN the number of simple molecules of water in the shell between r and r+dr is given by $\frac{k'}{r^n}$ (it makes sense because if the molecules is far from the core there is practically no chance to stick to the liquid droplet) , k' is a constant real. With the same method we can write

$$dN = \frac{k'}{r^n}(4\pi r^2)dr \tag{41}$$

By integration, one obtains

$$N = \int_a^{\infty} \frac{k'}{r^n}(4\pi r^2)dr \tag{42}$$

Thus the number of water molecules that can be fixed by the isolated liquid droplet is

$$N = \frac{4\pi k'}{(n-3)} a^{(3-n)} \tag{43}$$

Also

$$\frac{dN}{N} = df_n(r) = \Pi_n(r)dr \tag{44}$$

With

$$\Pi_n(r) = (n-3)\,\frac{a^{n-3}}{r^{n-2}} \tag{45}$$

for $r \geq a$

and

$$\bar{r} = \int_a^{\infty} r\Pi_n(r)dr = \frac{(n-3)}{(n-4)}\,a \tag{46}$$

which is valid for $n>4$

See Fig. B-3 for the distribution function

$$\frac{dr}{dt} = \frac{1}{\Pi_n(\bar{r})}\,\frac{df_n(\bar{r})}{dt} \tag{47}$$

$$\frac{df_n(\bar{r})}{dt} = \frac{d}{dt}\ln\frac{4\pi(\bar{r})^3}{3} = \frac{3}{r^*}\,\frac{dr^*}{dt} \tag{48}$$

$$\frac{dr}{dt} = \frac{3}{n-3}\,\frac{(\bar{r})^{n-2}}{(r^*)^{n-2}}\,\frac{dr^*}{dt} = 3\,\frac{dr^*}{dt}\,\frac{1}{n-3}\left(\frac{n-3}{n-4}\right)^{n-2} \tag{49}$$

$$\frac{dr^*}{dt} = -\frac{(r^*)^2}{A}\,\frac{d}{dt}\ln P \tag{50}$$

Then

$$\frac{dr}{dt} = hs(t) \tag{51}$$

where h is the growth factor independent of time due to the proposed

mechanism.

$$h = 3\,\frac{(n-3)^{n-3}}{(n-4)^{n-2}} \tag{52}$$

and $s(t)$ is the time evolution

$$s(t) = -\frac{(r^{*})^{2}}{A}\frac{d}{dt}\ln P \tag{53}$$

We can, express the radius evolution as follows

$$r(t,t_0) = r^{*}(t_0) - hA\int_{t_0}^{t}\frac{d(\ln P(t))}{\left[\ln\frac{P}{P_\infty}\right]^{2}} \tag{54}$$

or

$$r(t,t_0) = r^{*}(t_0) + hA\left[\frac{1}{\ln\frac{P(t)}{P_\infty}} - \frac{1}{\ln\frac{P(t_0)}{P_\infty}}\right] \tag{55}$$

Where

P_∞ is given by the Clausius - Clapeyron law (1)

And one can write the evolution of the radius in the following form

$$r(t,t_0) = r^{*}(t_0) + h\,(r^{*}(t) - r^{*}(t_0)) \tag{56}$$

Application for the non-equilibrium flows

The growth rate of the droplet is

$$\frac{dl}{dt} = 4\pi\rho_c \left[\frac{I(t)(r^*(t_0))^3}{3\rho(t)} + \frac{dr}{dt} \int_0^t \frac{I(\tau)}{\rho(\tau)} \left[r(\tau, \tau_0) \right]^2 d\tau \right] \tag{57}$$

where

$$r(\tau, \tau_0) = r^*(\tau_0) + h\,(r^*(\tau) - r^*(\tau_0)) \tag{58}$$

and $l(t)$ is obtained by integration.

What is usually calculated is the variation with time for a given particle path of

a) the nucleation rate I

b) the number density of critical clusters (droplets) which is

$$N^* = \frac{4}{3}\pi r^{*3} \frac{\rho_c}{\mu}$$

c) $\frac{dl}{dt}$ is the condensation rate

d) l the condensate mass fraction

VI - Discussion

We have presented a theory of homogeneous nucleation of gases, which can be applied to equilibrium and nonequilibrium conditions. The growth rate is no more a constant as in the classical Becker-Doring theory [6]. In our theory

the growth rate is time dependent according to two different models : the soft core model and the hard core model.

In some phenomena related to droplet growth as dew formation[10], it has been found successively after the critical size has been reached the following law

$$\frac{dr}{dlnt} \sim t^{1/3} \quad \text{(for t small)}$$

It was interpreted as isolated growth without coalescence, then

$$\frac{dr}{dlnt} \sim t^{1/2} \quad \text{(for medium range of t)}$$

It was interpreted as growth with coalescence in one dimension. Finally

$$\frac{dr}{dlnt} \sim t \quad \text{(for t large)}$$

This last case was interpreted as growth with coalescence in two dimensions (the usual linear growth law of classical theory). These successive laws were found experimentally and through computer simulations. We can use our theory to explain with one unified reasoning the peculiar behavior of dew formation which is also encountered in thin film growth [11]. This is the object of future research projects.

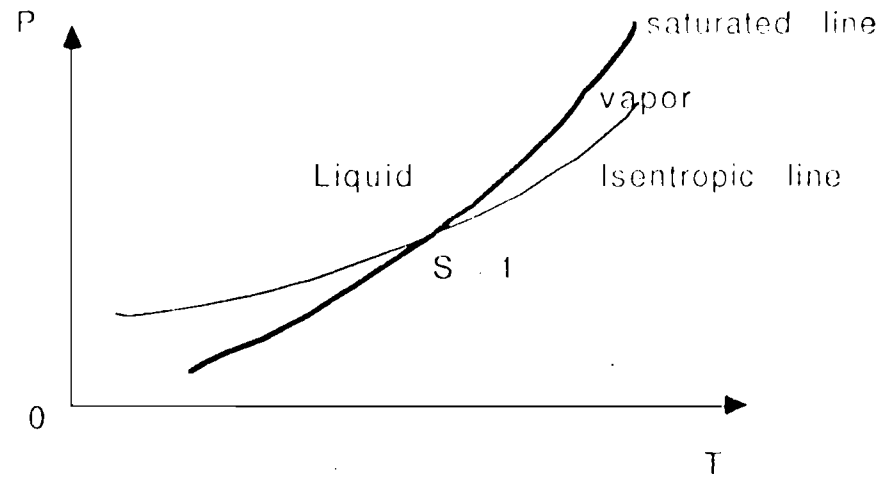

Figure B-1 : P,T diagram

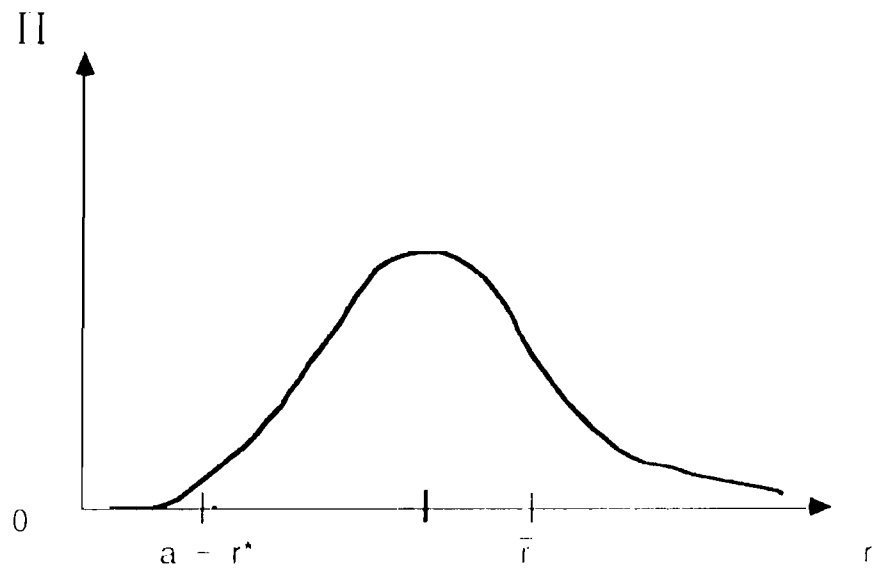

Figure B-2 : The distribution function

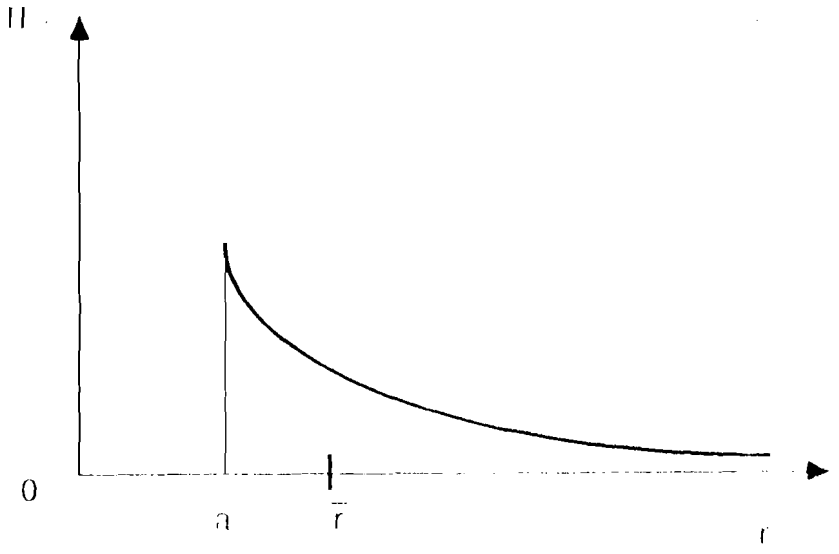

Figure B-3 : The distribution function (hard core model)

References

[1]- J.P. Sislian and I.I. Glass , Condensation of water vapor in rarefaction waves : I. Homogeneous nucleation , AIAA journal ,dec 1976

[2] - Dieter Barschdorff ; Carrier gas effects on homogeneous nucleation of water vapor in shock tube ; Phy.fluids , vol. 18, 529, 1975

[3] - J.A. Johnson ,III, L.E. Johnson , and X.N. Lu ; Turbulence in a reacting contact surface ; Phy.fluids ;vol. 2, 2002, 1990

[4] - Upul de Silva and Joseph A. Johnson III (submitted to publication 1994)

[5] - Peter P. Wegener ; Gasdynamics of expansion flows with condensation and homogeneous nucleation of water vapor; in "Nonequilibrium Flows" edited by P.P. Wegener , Marcel Dekker, NY 1969

[6] - A.C. Zettlemoyer , Nucleation; 1969; edited by A.C. Zettlemoyer, (Dekker, New-York)

[7] - Becker, R. and Doring , W, Ann.Phys. 24, 719(1935)

Penrose,O. , in "Stochastic processes in Nonequilibrium systems " (L. Garrido ,P. Seglar and P.J. Shepherd,eds) Lecture notes inPhysics vol.84, Springer Verlag ,Berlin 1978

[8] - Langer ,J.S. , in "Systems far from equilibrium" (L. Garrido , ed.) Lecture notes inPhysics, vol. 132,Springer Verlag, Berlin , 1980

[9] - S. Chandrasekhar : Rev. Mod . Phys. 15, 1 (1943)

[10] - J.L. Viovy et al ; Phys. Rev.;A37,4965,1988

[11] - B. Brisco and K. Galvin ; Growth with coalescence during condensation Phys. rev . A43, 1900, 1991